https://doi.org/10.5194/acp-2020-1130
Preprint. Discussion started: 17 November 2020

Atmospheric Chemistry and Physics Discussions

Organic pollutants from tropical peatland fires: regional influences and its impact on lower stratospheric ozone

Simon Rosanka[1], Bruno Franco[2], Lieven Clarisse[2], Pierre-François Coheur[2], Andreas Wahner[1], and Domenico Taraborrelli[1]

[1]Institute of Energy and Climate Research, IEK-8: Troposphere, Forschungszentrum Jülich GmbH, Jülich, Germany
[2]Spectroscopy, Quantum Chemistry and Atmospheric Remote Sensing (SQUARES), Université libre de Bruxelles (ULB), Brussels 1050, Belgium

Correspondence: Simon Rosanka (s.rosanka@fz-juelich.de)

Abstract. The particularly strong dry season in Indonesia in 2015, caused by an exceptional strong El Niño, led to severe peatland fires resulting in high volatile organic compound (VOC) biomass burning emissions. At the same time, the developing Asian monsoon anticyclone (ASMA) and the general upward transport in the intertropical convergence zone (ITCZ) efficiently transported the resulting primary and secondary pollutants to the upper troposphere/lower stratosphere (UTLS). In this study, we assess the importance of these VOC emissions for the composition of the lower troposphere and the UTLS, and we investigate the effect of in-cloud oxygenated VOC (OVOC) oxidation during such a strong pollution event. This is achieved by performing multiple chemistry simulations using the global atmospheric model ECHAM/MESSy (EMAC). By comparing modelled columns of the biomass burning marker hydrogen cyanide (HCN) to spaceborne measurements from the Infrared Atmospheric Sounding Interferometer (IASI), we find that EMAC properly captures the exceptional strength of the Indonesian fires.

In the lower troposphere, the increase in VOC levels is higher in Indonesia compared to other biomass burning regions. This has a direct impact on the oxidation capacity, resulting in the largest regional reduction in hydroxyl radicals (OH) and nitrogen oxides (NO_x). Even though an increase in ozone (O_3) is predicted close to the peatland fires, particular high concentrations of phenols lead to an O_3 depletion in eastern Indonesia. By employing the detailed in-cloud OVOC oxidation scheme Jülich Aqueous-phase Mechanism of Organic Chemistry (JAMOC), we find that the predicted changes are dampened and that by ignoring these processes, global models tend to overestimate the impact of such extreme pollution events.

In the ASMA and the ITCZ, the upward transport leads to elevated VOC concentrations in the UTLS region, which results in a depletion of lower stratospheric O_3. We find that this is caused by a high destruction of O_3 by phenoxy radicals and by the increased formation of NO_x reservoir species, which dampen the chemical production of O_3. The Indonesian peatland fires regularly occur during El Niño years and contribute to the depletion of O_3. In the time period from 2001 to 2016, we find that the lower stratospheric O_3 is reduced by about 0.38 DU and contributes to about 25 % to the lower stratospheric O_3 reduction observed by remote sensing. By not considering these processes, global models might not be able to reproduce this variability in lower stratospheric O_3.

https://doi.org/10.5194/acp-2020-1130
Preprint. Discussion started: 17 November 2020

Atmospheric Chemistry and Physics Discussions

1 Introduction

Particularly strong Indonesian wildfires during the El Niño in 2015 led to severe air pollution and reduced visibility (Kim et al., 2015; Lee et al., 2017) resulting in increased morbidity and mortality (Marlier et al., 2013; Reddington et al., 2014; Crippa et al., 2016) in South-East Asia (SEA). In general, El Niño is a large-scale climate anomaly, which is characterised by significantly warmer eastern equatorial Pacific Ocean sea surface temperatures (Trenberth, 1997), resulting in a dry season in SEA (Weng et al., 2007). The very strong El Niño phase in 2015-2016, which is the third strongest on record (after 1997–1998 and 1982–1983, NOAA, 2020), led to a particularly strong dry season in Indonesia (Jiménez-Muñoz et al., 2016). In the past, much of the originally forested and moist peatland in Kalimantan and Sumatra has been drained and cleared during agricultural land management. In order to clear these forests, landscape fires are commonly used. Even small local fires in these regions during non El Niño years may induce particular strong biomass burning emissions. Gaveau et al. (2014) estimate that a local one-week Indonesian biomass burning event in 2013 contributed to about 5-10 % of Indonesian's total greenhouse gas emissions in that year. The additional drying during El Niño years favours fires that burn deep down into the peat and can last for multiple weeks. Due to their long lifetimes, these fires spread and ignite new areas, which are not necessarily prone to biomass burning. Compared to non El Niño years, this results in strong biomass burning emissions from Indonesia (van der Werf et al., 2017). The underground conditions inherently determine smouldering fires, which are characterised by low combustion temperatures. In combination with the high carbon content of peat, this smouldering fires emit much larger amounts of non-CO_2 emissions from peatlands than from other fuels (Christian et al., 2003; Rein et al., 2009; Yu et al., 2010). A major fraction of these non-CO_2 emissions are volatile organic compounds (VOCs), which comprise a large variety of species influencing atmospheric chemistry on a regional and global scale. In the atmosphere, VOCs mainly react with the hydroxyl radical (OH), ozone (O_3), and the nitrate radical (NO_3), or photodissociate. Their atmospheric lifetimes range from minutes to years. Figure 1 shows the dry matter burned (DMB) during the 2015 Indonesian fires along the distribution of the peatlands (indicated in blue). It becomes evident that most of the areas influenced by biomass burning (e.g. Sumatra, Kalimantan) are covered with peatland, indicating that the 2015 Indonesian fires are characterised by high VOC emissions.

During the Indonesian biomass burning season, usually the Asian monsoon is ongoing such that a large anticyclone spanning from tropical to temperate regions (from about 10° N to 40° N) evolves. This almost stationary globally prevailing meteorological pattern typically extends from the Middle East to Asia in the upper troposphere and lower stratosphere (UTLS) (Basha et al., 2020). As a convective system, the Asian monsoon anticyclone (ASMA) acts as pollution pump facilitating a fast transport of surface emissions to the UTLS (Park et al., 2008; Randel et al., 2010; Lelieveld et al., 2018). Vogel et al. (2015) analysed the impact of different regions in Asia on the chemical composition of the 2012 ASMA by using a chemical Lagrangian model. They found that air masses from SEA contribute significantly to the composition of the anticyclone in the UTLS. In addition, the vertically convective transport in the Inter Tropical Convergence Zone (ITCZ) and in the south-eastern flank of the anticyclone carries air masses from SEA into the UTLS. Thus, even short-lived VOCs from Indonesian fires are transported into the UTLS and potentially affect the lower stratospheric composition.

https://doi.org/10.5194/acp-2020-1130
Preprint. Discussion started: 17 November 2020

Atmospheric Chemistry and Physics Discussions

The Asian monsoon is characterised by the frequent occurrence of clouds and precipitation, and it has been demonstrated that the ASMA has a higher water vapour content than usual systems (Fu et al., 2006). At the same time, the Madden–Julian Oscillation (MJO) leads to enhanced water vapour concentrations and precipitation over the Indian Ocean and Indonesia (Zhang, 2013). Many oxygenated VOCs (OVOCs) have a high solubility and quickly partition and react in cloud droplets influencing radical concentrations and the atmospheric composition in general (Herrmann et al., 2015). Rosanka et al. (2020b) showed that the in-cloud OVOC oxidation has a significant impact on the predicted concentrations of VOCs, key oxidants, and O_3. In the past, global atmospheric chemistry models were not capable to represent this process explicitly nor in its full complexity (Ervens, 2015). However, the recently developed Jülich Aqueous-phase Mechanism of Organic Chemistry (JAMOC, Rosanka et al., 2020c,b) comprises an advanced in-cloud OVOC oxidation scheme suitable to be used in the ECHAM/MESSy Atmospheric Chemistry (EMAC, Jöckel et al., 2010) model. This allows us to assess the importance of this in-cloud oxidation process during the VOC-dominated Indonesian peatland fires.

In this study, we therefore investigate the importance of biomass burning VOC emissions from the strong 2015 Indonesian peatland fires on the (1) lower tropospheric composition, (2) the importance of in-cloud OVOC oxidation in such an extreme pollution event, and (3) the influence of the emitted VOCs on the UTLS. In addition to the 2015 fires, strong peatland fires frequently occur in Indonesia. Especially during El Niño years (in 2002–2003, 2004–2005, 2006–2007, 2009–2010, and 2014-2016), high emissions have been observed (van der Werf et al., 2017). Therefore, the long-term impact of these periodicaly occurring events is additionally addressed. Globally, biomass burning is not limited to Indonesia and many regions are frequently affected. In each region, biomass burning varies in strength, frequency, the characteristics of the biomass burned, and the chemical background conditions. Peatland only covers about 2.84 % of the Earth's land mass (Xu et al., 2018) making equatorial Asia the region where most peatland is burned. Since non-peatland biomass burning emissions result in lower VOC emissions (Akagi et al., 2011), Indonesia is characterised by a unique emission footprint. In order to address the resulting differences to other biomass burning dominated regions, we compare the influence to seven regions with high biomass burning emissions. Figure 2 and Table 1 provide an overview of each region. This approach also allows us to analyse the global impact of all biomass burning VOC emissions on the atmospheric composition. Figure 3 shows the relative contribution of each region to the 2015 total biomass burning emissions of VOCs and aromatics, a subgroup of VOCs. These emissions are calculated based on dry matter combustion rates from the Global Fire Assimilation System (GFAS) and emission factors from Akagi et al. (2011) (for further details see Sect. 2.1.2). Due to the unique emission footprint from the Indonesian fires, SEA contributes 30 % of the total biomass burning VOC emissions and more than $1/3$ to the total aromatic emissions. The two northern regions Alaska (ALA) and North Asia (NAS), which are characterised by extratropical forest with organic soil, add significantly to the global VOC emissions from biomass burning, even though their contribution to the total burned mass is low. The highest total emissions of almost 40 % originate from Central Africa (CAF) and South Africa (SAF). This is twice as much as from SEA but since mainly tropical forest and savanna are burned, the contribution to the total biomass burning attributed to aromatic emissions is only half, when compared to SEA. The two regions dominated by savanna, Central South America (CSA) and North Australia (NAU), contribute the least to the VOC emissions.

https://doi.org/10.5194/acp-2020-1130
Preprint. Discussion started: 17 November 2020

Atmospheric Chemistry and Physics Discussions

The importance of biomass burning VOC emissions is addressed by performing multiple global chemistry simulations using the ECHAM/MESSy Atmospheric Chemistry (EMAC, Sect. 2) model. In a first step, the ability of EMAC to represent biomass burning events is evaluated using hydrogen cyanide (HCN) satellite retrievals (Sect. 3). Afterwards the impact of the 2015 Indonesian peatland fires on the lower troposphere (Sect. 4) is analysed, focusing on VOCs and key radicals. Some VOCs are known to be toxic of which some are emitted or formed from biomass burning. They might have a significant influence on the Indonesia's population, which is the World's fourth highest (United Nations, 2019). Therefore, a selection of toxic species is additionally analysed in this section. Sect. 5 and Sect. 6 discuss the importance of in-cloud OVOC oxidation during this pollution event and the influence on the UTLS, respectively. Modelling uncertainties related to this study are discussed in Sect. 7 before drawing final conclusions (Sect. 8).

2 Modelling approach

This section provides an overview on the global model used in this study. The main focus is placed on the representation of atmospheric gas- and aqueous-phase chemistry, biogenic and biomass burning emissions, and the strategy to compare EMAC's prediction to satellite retrievals (Sect. 2.1). Sect. 2.2 provides an overview of each simulation performed in this study.

2.1 EMAC

The ECHAM/MESSy Atmospheric Chemistry (EMAC) model is a numerical chemistry and climate simulation system that includes submodels describing tropospheric and middle-atmosphere processes and their interaction with oceans, land, and human influences (Jöckel et al., 2010). It uses the second version of the Modular Earth Submodel System (MESSy2) to link multi-institutional computer codes. The core atmospheric model is the 5th-generation European Centre Hamburg general circulation model (ECHAM5, Roeckner et al., 2006). Jöckel et al. (2010) provide an update on all modelling components used. For the present study, we applied EMAC (ECHAM5 version 5.3.02, MESSy version 2.54.0) in the T106L90MA and T42L90MA resolution, i.e. with a spherical truncation of T106 and T42 (corresponding to a quadratic Gaussian grid of approximately 1.1° by 1.1° and 2.8° by 2.8°, respectively). By using this horizontal resolution, addressing the short-term implications for 2015–2016 as well as the long-term impact (2001–2016) on a global scale is still feasible while at the same time, the computational costs are affordable. For both resolutions, 90 vertical hybrid pressure levels up to 0.01 hPa (focusing on the lower and middle atmosphere) are used, representing tropospheric and stratospheric transport processes reasonably well (Jöckel et al., 2010). Thus, the impact on the troposphere and the UTLS can be addressed. A detailed discussion on the comparability of both resolutions is performed in Sect. 7.

2.1.1 Atmospheric chemistry

Within this study, the gas- and aqueous-phase chemistry is modelled by two separate submodels. For the atmospheric gas-phase chemistry, the applied model setup comprised the submodel Module Efficiently Calculating the Chemistry of the Atmosphere (MECCA, Sander et al., 2019) using the gas-phase Mainz Organic Mechanism (MOM). MOM contains an extensive oxidation

https://doi.org/10.5194/acp-2020-1130
Preprint. Discussion started: 17 November 2020

scheme for isoprene (Taraborrelli et al., 2009, 2012; Nölscher et al., 2014), monoterpenes (Hens et al., 2014), and aromatics (Cabrera-Perez et al., 2016) and is therefore capable to represent all the biomass burning VOCs considered in EMAC. In addition, comprehensive reactions schemes are considered for the modelling of the chemistry of NO_x ($NO+NO_2$), HO_x ($OH+HO_2$), CH_4 and anthropogenic linear hydrocarbons. VOCs are oxidised by OH, O_3, and NO_3, whereas peroxy radicals (RO_2) react with HO_2, NO_x, and NO_3, and undergo self- and cross-reactions (Sander et al., 2019). Isocyanic acid (HNCO) is a chemical constituent that is heavily emitted by biomass burning and potentially harmful to humans (Wang et al., 2007; Roberts et al., 2011; Leslie et al., 2019). In order to properly represent this toxic constituent within EMAC, MOM has been extended to represent the atmospheric chemistry of HNCO. For this, the mechanism proposed by Rosanka et al. (2020d) is implemented into MOM. Their mechanism includes formamide as an additional chemical source of HNCO and chemical mechanisms for nitromethane, methylamine, dimethylamine, and trimethylamine.

The atmospheric aqueous-phase chemistry is modelled using the SCAVenging submodel (SCAV, Tost et al., 2006). It simulates the removal of trace gases and aerosol particles by clouds and precipitation. SCAV calculates the transfer of species into and out of rain and cloud droplets using the Henry's law equilibrium, acid dissociation equilibria, oxidation-reduction reactions, heterogeneous reactions on droplet surfaces, and aqueous-phase photolysis reactions (Tost et al., 2006). As mentioned earlier and as demonstrated by Rosanka et al. (2020b), in-cloud OVOC oxidation significantly influences the atmospheric composition. However, the ordinary differential equations (ODE) systems resulting from the combination of gas-phase and in-cloud aqueous-phase suffer from (1) a higher stiffness due to fast acid-base equilibria and phase-transfer reactions, and (2) load imbalance on High-Performance Computing (HPC) systems due to the sparsity of clouds. This leads to a significant increase in computational costs when using larger chemical mechanisms like the Jülich Aqueous-phase Mechanism of Organic Chemistry (JAMOC), i.e. larger ODE systems (Rosanka et al., 2020c). Using JAMOC in each simulation performed in this study is thus not feasible. As a trade-off, JAMOC is used in a simulation subset in order to address and estimate its implications on the other simulations. Thus, two different aqueous-phase mechanisms are used within this study: (1) the standard aqueous-phase mechanism of EMAC (in the following called ScSta), which includes a detailed oxidation scheme and represents more than 150 reactions (Jöckel et al., 2016), and (2) JAMOC (Rosanka et al., 2020c), which includes a complex in-cloud OVOC oxidation scheme. In JAMOC, the phase transfer of species containing up to ten carbon atoms and the oxidation of species containing up to four carbon atoms are represented. Similar to MOM, both aqueous-phase mechanisms are modified to include the changes proposed by Rosanka et al. (2020d) to properly represent HNCO.

2.1.2 Biogenic and Biomass Burning VOC Emissions

In the atmosphere, biogenic and biomass burning emissions are the dominant sources of VOCs. The largest biogenic emissions take place in the equatorial region (e.g. Amazon Basin, Central Africa) with additional emissions in the Northern (NH) and Southern Hemisphere (SH) extratropics. The MESSy submodel Model of Emissions of Gases and Aerosols from Nature (MEGAN, Guenther et al., 2006) is used to calculate biogenic VOC emissions. The global emissions of isoprene, the most abundant biogenic VOC, are scaled to 595 $\mathrm{Tg\ a^{-1}}$, the best estimate of Sindelarova et al. (2014).

https://doi.org/10.5194/acp-2020-1130
Preprint. Discussion started: 17 November 2020


Atmospheric Chemistry and Physics Discussions

Biomass burning emission fluxes are calculated using the MESSy submodel BIOBURN, which determines these fluxes based on biomass burning emission factors and dry matter combustion rates. For the latter, data from the GFAS are used that are based on satellite observations of the fire radiative power obtained from the Moderate Resolution Imaging Spectroradiometer (MODIS) satellite instruments (Kaiser et al., 2012). In BIOBURN, the emission strength depends on the dominant fire type in the respective area. From the GFAS dataset used in EMAC, in 2015, the dominant fire type over Indonesia is tropical forest fire. However, as discussed earlier, peatland fires contribute substantially to the Indonesian fires. The GFAS dataset of EMAC is changed such that the dominant fire type over Indonesia is a combination of peat and tropical forest fires with equal contributions (following van der Werf et al., 2017). In general, biomass burning emission factors for VOCs are based on Akagi et al. (2011). Biomass burning emissions for HNCO, formamide, nitromethane, methylamine, dimethylamine, and trimethylamine are implemented following Rosanka et al. (2020d) using emission factors from Koss et al. (2018) for HNCO and formamide.

2.1.3 Observational comparison

The evaluation of model simulation results against global observational datasets of VOC abundance can be performed for only a few species, mainly because of the limited availability in spaceborne measurements of such compounds. Among them, several VOCs are retrieved globally from the observations made by the nadir-viewing hyperspectral Infrared Atmospheric Sounding Interferometer (IASI, Clerbaux et al., 2009). Embarked on the Metop platforms on sun-synchronous polar orbits, IASI crosses the equator at 9:30 and 21:30 local solar time and achieves a global coverage twice daily with a fairly dense spatial sampling. Although significant enhancements of carbon monoxide (CO) and ammonia (NH_3) have already been captured by the IASI measurements in the 2015 Indonesian fires (Whitburn et al., 2016b; Nechita-Banda et al., 2018), here we make use of the HCN abundance retrieved from the IASI/Metop–A and –B observations to assess the ability of EMAC to represent such an important biomass burning event. This choice is explained in Sect. 3. In addition, IASI methanol (CH_3OH) data are used to assess the impact of in-cloud OVOC oxidation in the model simulations (Sect. 5).

The retrieval method used to obtain the HCN measurements from the IASI observations follows closely the version 3 of the Artificial Neural Network for IASI (ANNI), which already allowed the retrieval of a suite of VOCs, including CH_3OH (Franco et al., 2018). ANNI is a general retrieval framework that consists in quantifying, for each IASI observation, the spectral signature of the target gas with a sensitive hyperspectral metric, and in converting this metric into gas total column via an artificial feedforward neural network (NN). Details on the ANNI retrieval approach, the HCN retrieval specificities, and the HCN product itself are provided in Appendix A. We refer to Franco et al. (2018) for a description of the IASI methanol retrievals. The satellite datasets exploited in this study consist of daily global distributions of HCN and CH_3OH total columns derived from the daytime observations (approximately 9:30 $a.m.$, local time) of the IASI/Metop–A and –B overpasses. These offer a better measurement sensitivity than the evening overpasses (Franco et al., 2018). Scenes affected by clouds or poor retrieval performance are removed from the final dataset by specific filters. Examples of daily regional distributions of HCN columns in the 2015 Indonesian fires as well as the seasonal global distributions of HCN as retrieved from IASI are presented

https://doi.org/10.5194/acp-2020-1130
Preprint. Discussion started: 17 November 2020


Atmospheric Chemistry and Physics Discussions

in Appendix A. Those highlight the ability of IASI to capture the enhancements of HCN during biomass burning events as well as its downwind transport over long distances.

2.2 Simulations performed

Within this study, seven simulations are performed, which can be summarised in three simulation sets. Each simulation differs either in the biomass burning emissions, the aqueous-phase mechanism used, or the modelled time period. Table 2 provides an overview of all simulations and their characteristics. For each simulation set, one simulation exists, in which all VOC emissions from biomass burning are switched off (named REF and $\mathrm{REF_{LONG}}$). A second simulation includes biomass burning VOC emissions as described in Sect. 2.1.2 (named FIR and $\mathrm{FIR_{LONG}}$). Performing high resolution simulations with the highest complexity in the chemical mechanisms in EMAC comes with high computational costs. The strong Indonesian peatland fires of 2015 and the following year are selected as a specific case study (named REF and FIR). For both simulations, the year 2014 is simulated as spin up, which is not considered for the analysis. For this case study, high resolution simulations are performed at T106L90MA. In order to isolate the impact of the Indonesian peatland fires in 2015, an additional simulation (named $\mathrm{FIR_{NOINDO}}$) is performed, for which all biomass burning VOC emissions from Indonesia are switched off. In order to address the impact of in-cloud OVOC oxidation on such VOC-dominated pollution event, two simulations including JAMOC are performed (named $\mathrm{REF_{JAMOC}}$ and $\mathrm{FIR_{JAMOC}}$). However, to reduce the computational demand (see Sect. 2.1.1), these simulations focus only on the second half of 2015 at T106L90MA resolution. The long-term effect of reoccurring Indonesian peatland fires are addressed by performing two long simulations for the time period of 2001–2016 (named $\mathrm{REF_{LONG}}$ and $\mathrm{FIR_{LONG}}$). Here, the year 2000 is simulated for spin up, which is not used for the analysis. Performing these simulations at T106L90MA and using JAMOC is computationally not feasible. Therefore, the EMAC's standard aqueous-phase mechanism is used and the resolution is reduced to T42L90MA.

3 The representation of biomass burning events in EMAC

HCN mainly originates from combustion processes and is therefore largely emitted by biomass burning (Shim et al., 2007). Other emission sources including industrial activities, automobile exhaust, and domestic biofuel are assumed to be very weak (Lobert et al., 1990; Li et al., 2009). Reactions involving acetonitrile ($\mathrm{CH_3CN}$) are the only gas-phase source of HCN, but those are estimated to be a minor contribution to the atmospheric HCN burden (Li et al., 2009). The slow oxidation of HCN by OH and $\mathrm{O(^1D)}$ is considered to be the most important atmospheric gas-phase sink, leading to long chemical lifetimes (Cicerone and Zellner, 1983). However, due to a strong ocean uptake, the atmospheric lifetime is reduced to a few months (Li et al., 2000, 2009). The almost exclusive biomass burning source, combined with a long atmospheric residence time that allows for long-range transport, makes HCN a widely used primary tracer of biomass burning emissions and fire plumes (Li et al., 2009). Other typical fire tracers such as CO and $\mathrm{NH_3}$ either have several other sources or are too short-lived to track fire plumes over long distance. Therefore, HCN satellite data from IASI are used here to evaluate the performance of EMAC in representing the 2015 Indonesian peatland fires.

https://doi.org/10.5194/acp-2020-1130
Preprint. Discussion started: 17 November 2020


Atmospheric Chemistry and Physics Discussions

Figure 4 shows the comparison of modelled HCN total columns to IASI satellite retrievals for the three months with strong peatland emissions in Indonesia. At the beginning of the Indonesian fires, the emitted HCN is transported westwards leading to high HCN column values over the Indian Ocean. While the fires are ongoing throughout October, the strong westward transport of HCN results in the complete covering of the Indian ocean. Some HCN is also transported eastwards over Australia and the Pacific Ocean. In November, the air masses from Indonesia mix with emissions from Africa and the eastward transported air masses reach South America. In general, EMAC strongly underestimates HCN when its biomass burning source is not taken into account (simulation REF). Once the HCN biomass burning emissions are taken into account, the overall underprediction in EMAC is mostly resolved. However in the FIR simulation, HCN is partially overpredicted in SEA during the main fire period (September and October). Additionally, HCN columns are slightly overestimated in CSA (September and October) and CAF (September). Interestingly, the relative model bias (not shown) is similar in all three regions. Due to the particular strength of the Indonesian fires, the absolute bias is more pronounced in SEA. EMAC's representation of HCN is associated with some uncertainties. The occurrence of biomass burning events is very low in the Amazon Basin, suggesting that the high HCN column values are not caused by fires or transport from CSA. Especially in NH autumn (SON), the Amazon basin is known to be highly influenced by biogenic emissions. Shim et al. (2007) already suggested that biogenic HCN emissions may contribute to atmospheric concentrations by up to 18 %. In the submodule MEGAN, biogenic HCN emissions are taken into account and contribute about 15 % to the total HCN emissions, suggesting that EMAC's overprediction is not caused by a misrepresentation of other sources. Additionally, it is expected that the atmospheric lifetime of HCN is reasonably well represented, since globally HCN columns are well reproduced. Moreover, the ocean uptake accounts for 1.2 $\mathrm{Tg(N)\,a^{-1}}$, which is well in the range of 1.1 to 2.6 $\mathrm{Tg(N)\,a^{-1}}$ proposed by Li et al. (2000) and very close to the Singh et al. (2003) estimate of 1.0 $\mathrm{Tg(N)\,a^{-1}}$. The representation of biomass burning within EMAC depends on satellite observations (Sect. 2.1.2), which retrieve the fire radiative power and are thus sensitive to clouds. This introduces some uncertainties in regions that are characterised by the frequent occurrence of clouds, like equatorial Asia. Focusing on Indonesia, Liu et al. (2020) compared five different global fire inventories and found that GFAS, the inventory used in this study, represents the strength of these fires best. Still, GFAS even tends to slightly underestimate the strength, when compared to regional observations in Singapore, Malaysia, and Indonesia. This suggests that the magnitude of the Indonesian fires is well represented in EMAC. In this study, we use the emission factors optimised for atmospheric models by Akagi et al. (2011), which suggest 5.0 $\mathrm{g\,kg^{-1}}$ for HCN from peatland fires. However, from the literature a high uncertainty in the emission factors for HCN are reported. From recent field measurements in Indonesia and Malaysia, Stockwell et al. (2016) and Smith et al. (2018) report values ranging from 0.34 $\mathrm{g\,kg^{-1}}$ to 8.21 $\mathrm{g\,kg^{-1}}$, whereas lab measurements for Indonesian peatland by Stockwell et al. (2015) suggest values between 3.30 $\mathrm{g\,kg^{-1}}$ and 3.83 $\mathrm{g\,kg^{-1}}$. Overall, this results in a mean emission factor of 4.40 $\mathrm{g\,kg^{-1}}$ across all studies (Andreae, 2019), suggesting that some of EMAC's overestimation is caused by a slightly too high HCN emission factor. Due to its long lifetime, HCN is transported over long distances. West of Indonesia, EMAC also predicts higher HCN columns than observed by IASI, suggesting that some of the overprediction is caused by the deviation of horizontal transport (further discussed in Sect. 7). Figure 5 gives the frequency of the global HCN EMAC total column bias in relation to the IASI retrievals during the Indonesian peatland fires, once including biomass burning emissions in the simulations and once not. This comparison confirms

https://doi.org/10.5194/acp-2020-1130
Preprint. Discussion started: 17 November 2020


Atmospheric Chemistry and Physics Discussions

that HCN is strongly underestimated when its main source is not represented in EMAC. With HCN from biomass burning, the mean column bias reduces from -5.32×10^{-15} molecules cm^{-2} to -1.06×10^{-15} molecules cm^{-2} and its variance reduces from 1.75×10^{-31} molecules^2 cm^{-4} to 2.57×10^{-30} molecules^2 cm^{-4}, significantly improving the representation of HCN in EMAC. From this analysis we conclude that even though EMAC does not reproduce HCN columns perfectly, the Indonesian fires are reasonably well represented, especially when considering the exceptional strength of the 2015 Indonesian fires (for further discussion see Appendix A and Fig. A3). This also holds true considering all global biomass burning emission events.

4 The influence on the lower troposphere

In the following subsections, the impact of the 2015 Indonesian peatland fires on the lower tropospheric composition is analysed. In addition, substantial differences to the other six biomass burning dominated regions are discussed. All results are based on the simulations REF and FIR. Table 3 provides an overview on the global and regional changes (between simulation REF and FIR) in the tropospheric burden of each species discussed in the following subsections. The regional changes reported in Table 3 are calculated for the respective main biomass burning season defined in Table 1.

4.1 Impact on VOCs

Many VOCs are characterised by short lifetimes resulting in highly location-dependent changes within the troposphere. Direct emissions are the only source of atmospheric hydrocabons. Globally, biomass burning emissions of VOCs significantly increase the atmospheric concentration of many hydrocarbons, with acetylene (C_2H_2) and ethane (C_2H_6) being the two hydrocarbons impacted the most. Their tropospheric burden increases by 20.5 % and 32.6 %, respectively, with the highest regional change is in SEA.

The two most abundant aromatics, benzene (C_6H_6) and toluene (C_7H_8), are strongly emitted by biomass burning events. In the FIR simulation, the tropospheric burden of C_6H_6 increases by 27.3 %. Toluene has a slightly lower increase of only 15.3 %. The tropospheric concentration of oxygenated aromatics also increases strongly. The most dominant change is predicted for phenol (C_6H_5OH), whose tropospheric burden is more than doubled and increases to 2.3 Gg. Even though phenol is directly emitted by biomass burning, the overall high aromatic emissions lead to an enhanced chemical production of phenol from benzene oxidation. The highest absolute change is observed in SEA. However, due to low aromatic background concentrations, the relative increase is higher in ALA, CSA, and NAU.

Methanol (CH_3OH) is directly emitted by biomass burning emissions but also chemically produced from VOC oxidation. Globally, methanol increases by 7.9 % when biomass burning VOC emissions are taken into account. The high VOC emissions during the Indonesian peatland fires result in the highest changes in SEA. The two α-dicarbonyls glyoxal (OCHCHO) and methyl glyoxal ($CH_3C(O)CHO$) are primarily produced from VOC oxidation. The global burden of glyoxal and methyl glyoxal increases by 9.3 % and 1.3 %, respectively. Again, the highest absolute changes are predicted in SEA. However, the highest relative change occurs in ALA due to generally low background VOC concentrations.

https://doi.org/10.5194/acp-2020-1130
Preprint. Discussion started: 17 November 2020


Atmospheric Chemistry and Physics Discussions

In the atmosphere, organic acids are mainly produced from the photo-oxidation of biogenic and anthropogenic VOCs but may also be emitted from biomass burning. Formic acid (HCOOH) is slightly impacted by biomass burning VOC emissions and globally increases by 4.9 % with the highest changes in SEA and Africa (CAF and SAF). The acid impacted the most by biomass burning is acetic acid (CH_3CO_2H), which globally gains 23.3 % with the highest changes in SEA, CAF, CSA, and SAF. Interestingly, the high increase predicted in CSA only leads to a low relative rise. This is due to generally high background concentrations in this region from high biogenic VOC emissions.

4.2 Impact on hydroxyl radicals (OH)

In general, organic molecules react with OH by either H-abstraction or addition to double bonds, making OH the most important daytime VOC oxidant. Figure 6a gives the mean tropospheric surface OH concentration in 2015 and Fig. 6b presents the changes due to biomass burning VOC emissions. OH concentrations are significantly reduced in most regions with frequent biomass burning events. This reduction is caused by the direct reaction of OH with VOCs, and the enhanced formation of CO from VOC degradation. The reduction in OH is not uniformly distributed and depends on the local chemical regime. In Indonesia, the high VOC emissions lead to the highest absolute and relative OH reduction. The enhanced oxidation of VOCs by OH leads to an overall increase in HO_2. In ALA and NAS, the most northern areas of interest, the absolute change in OH is low. Within the biomass burning plume, the enhanced HO_2 concentrations react with NO producing OH and compensating the OH reduction by VOC degradation, resulting in a regional surface OH increase. Still, outside the biomass burning plume, an overall decrease in OH is predicted in ALA and NAS. Here, VOCs from biomass burning become the highest OH sink resulting in strong relative changes in OH reactivity. In general, OH reactivity is the highest in the Amazon Basin (100 s^{-1}) and the lowest in Antarctica (0.5 s^{-1}). The additional VOC emissions in Indonesia result in a significant increase of about 50 % in the OH reactivity, which is similar to the increases predicted in ALA and NAS.

4.3 Impact on nitrogen oxides (NO_x) and nitrate radicals (NO_3)

Figures 7a and 7b show the mean surface NO_x concentrations and the changes induced by the VOC biomass burning emissions, respectively. The additional VOC emissions significantly reduce the regional concentrations in tropospheric NO_x. In SEA, the absolute changes are large but small in relative (about 8 %), whereas the highest absolute and relative NO_x changes are predicted in ALA. These reductions are caused by enhanced reactions of RO_2 with NO_x resulting in an increased formation of NO_x reservoir species (i.e. alkyl and acyl peroxy nitrates) and nitrogen-containing aromatics (e.g. nitrophenols).

NO_3 is the most important nighttime oxidant, which is globally increased by about 5 %. On the one hand, the formation of NO_3 is enhanced from aromatic RO_2 reacting with NO_2, but on the other hand the loss of NO_3 by reactions with RO_2 and aldehydes is increased. In the two northern regions (ALA and NAS), the elevated O_3 and regionally increased NO_2 concentrations induce an enhanced formation from inorganic reactions, resulting in an additional rise of NO_3. The absolute increase in NO_3 is high in SEA, especially in Indonesia. Here, the particularly large increase in phenols results in enhanced concentrations of phenyl peroxy radicals ($C_6H_5O_2$), which form NO_3 when reacting with NO_2 following Jagiella and Zabel

https://doi.org/10.5194/acp-2020-1130
Preprint. Discussion started: 17 November 2020

Atmospheric Chemistry and Physics Discussions

(2007):

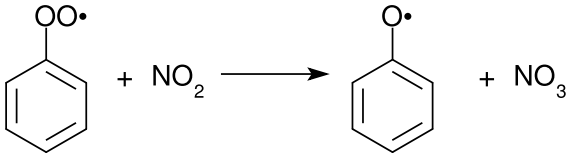

(R1)

Taraborrelli et al. (2020) recently studied the importance of aromatics on the atmospheric composition on a global scale. They also demonstrated the importance of this reaction but in opposition to this study, predicted a reduction of NO_3 in Indonesia. Taraborrelli et al. (2020) analysed 2010, a year with little biomass burning emissions in Indonesia (van der Werf et al., 2017), reducing the importance of this production channel.

4.4 Impact on ozone (O_3)

The perturbed NO_x–HO_x relation consequently leads to changes in tropospheric O_3. Figure 8a shows the mean tropospheric O_3 column and Fig. 8b illustrates the changes induced by VOC biomass burning emissions. Overall, EMAC predicts an enhanced formation of O_3. The increase in HO_2 leads to an enhanced chemical O_3 production by reacting with NO. Due to high NO_x emissions from biomass burning, the O_3 production is to a large extent VOC-limited. In the two northern regions, the background VOC concentrations are low resulting in the highest relative changes of more than 10 %. The same can be observed in Fig. 14b, which shows the zonal mean changes in the tropospheric O_3 column from 2001 onward. The largest changes are predicted in the NH high latitudes in 2003, a year with intense biomass burning in Boreal Asia (van der Werf et al., 2017). However, compared to the averaged tropospheric background O_3 concentrations, these changes are negligible on a global scale.

As described in Sect. 3, most VOC emissions from Indonesia are transported towards the Indian Ocean. Therefore, O_3 is predicted to increase in Sumatra and west of it (Fig. 8b). Interestingly, away from biomass burning emissions in Kalimantan and in east Indonesia, O_3 concentrations are slightly reduced, even though the chemical O_3 production still increases in this area. The decrease can also be observed in Fig. 14b during strong El Niño years, especially in 2006, 2009, 2014, and 2015. The particularly strong emissions of aromatics lead to enhanced concentrations of phenoxy radicals (C_6H_5O), which directly destruct O_3 (Tao and Li, 1999) in lower NO_x regions:

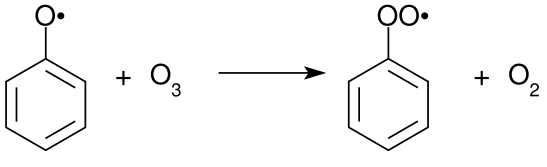

(R2)

This O_3 sink increases by 780 % resulting in a net loss of O_3 in these areas. Globally, this O_3 destruction channel gains from 144.9 to 200.1 $Tg\ a^{-1}$ in the troposphere. Also, Taraborrelli et al. (2020) reported a similar strength of this destruction channel of about 200 $Tg\ a^{-1}$. Therefore, biomass burning emissions regionally control the importance of this destruction channel.

https://doi.org/10.5194/acp-2020-1130
Preprint. Discussion started: 17 November 2020


Atmospheric Chemistry and Physics Discussions

4.5 Pollution and toxic conditions

The direct emission and degradation of primarily emitted VOCs lead to the formation of toxic compounds that are of special interest in highly populated areas. One prominent example is nitrophenols, which are known to have a high phytotoxic activity that is enhanced by a high photochemical stability (Grosjean, 1991). Rippen et al. (1987) and Natangelo et al. (1999) suggested that nitrophenols could have contributed to the forest decline in Northern and Central Europe in the 80's but also in other parts of the world. In the atmosphere, nitrophenols are mainly formed from the oxidation of the aromatic compounds benzene, toluene, phenols, and cresols (Nojima et al., 1975; Atkinson et al., 1980; Grosjean, 1984), of which the first three are emitted by biomass burning. Without aromatic biomass burning emissions, nitrophenol concentrations are only high in regions with high anthropogenic emissions (Fig. 9a). When biomass burning emissions of benzene, toluene, and phenols are included, nitrophenol concentrations significantly increase in areas affected by biomass burning. The strongest changes occur in SEA, CAF, and SAF (Fig. 9b). Many biomass burning regions frequently exceed nitrophenol thresholds that are determined for regions, where anthropogenic aromatic emissions dominate. On a global scale, biomass burning becomes the main source of nitrophenols, which have been measured in rain droplets (Leuenberger et al., 1985; Schummer et al., 2009). JAMOC represents the phase transfer of some nitrophenols. However, their reduction due to this additional sink is calculated to be below 1 %. This insignificant reduction results from the missing OH sink of these nitrophenols (Hems and Abbatt, 2018) in JAMOC. Therefore, the predicted nitrophenol concentrations are expected to be slightly overestimated. Still, the overall increase of nitrophenols in biomass burning areas is a potential danger for plants in these regions where plants are already under stressed conditions due to the biomass burning itself. At the same time, nitrophenols are known to absorb solar radiation (Hems and Abbatt, 2018) and therefore enhance hazy conditions in those areas (Lee et al., 2017), contributing to increased morbidity and mortality (Crippa et al., 2016).

Isocyanic acid (HNCO) is also known to be a toxic constituent of biomass burning emissions. It is linked to protein carbamylation, which causes adverse health effects such as rheumatoid arthritis, cardiovascular diseases, and cataracts (Wang et al., 2007; Roberts et al., 2011; Leslie et al., 2019). It is expected that the protein carbamylation potentially starts if humans are exposed to ambient concentrations above 1 ppb (Roberts et al., 2011). Rosanka et al. (2020d) already reported that HNCO concentrations are high in regions characterised by strong biomass burning events. Globally, similar high concentrations are predicted in this study. However, we predict higher concentrations in Indonesia than Rosanka et al. (2020d), who reported that ambient HNCO conditions of 1 ppb are exceeded for less than 30 days in Indonesia in 2011. The year 2011 is known to have low biomass burning emissions in this region (van der Werf et al., 2017). Figure 10 shows the number of days, in which this threshold is exceeded during the 2015 Indonesian peatland fires. Here, 1 ppb of HNCO is regularly exceeded and some regions are affected during the complete fire period. This causes potentially severe health effects for the population of Indonesia.

5 The influence of in-cloud OVOC oxidation during the Indonesian peatland fires

The influence of in-cloud OVOC oxidation is addressed by applying JAMOC during the Indonesian fire period (simulations $\mathrm{REF_{JAMOC}}$ and $\mathrm{FIR_{JAMOC}}$). In order to isolate the influence of the Indonesian peatland fires from the background changes

https://doi.org/10.5194/acp-2020-1130
Preprint. Discussion started: 17 November 2020

Atmospheric Chemistry and Physics Discussions

induced by JAMOC, the changes from the Indonesian fires due to the in-cloud OVOC oxidation are calculated following:

$$\Delta\mathrm{JAMOC} = (\mathrm{FIR}_{\mathrm{JAMOC}} - \mathrm{FIR}) - (\mathrm{REF}_{\mathrm{JAMOC}} - \mathrm{REF}) \quad (1)$$

Figure 11 shows the changes in the zonal mean concentration over Indonesia and the Indian Ocean of all OVOCs explicitly reacting in JAMOC for the simulations without JAMOC (Fig. 11a) and the predicted changes due to JAMOC (Fig. 11b; calculated using Reaction 1), focusing on the Indonesian fire period (SON). Due to the high solubility of many OVOCs and their in-cloud oxidation, their concentration is strongly reduced at altitudes that are characterised by frequent cloud events. The additional in-cloud sink for methanol, glyoxal, and methyl glyoxal leads to a lower increase in their burden ranging between 23 and 32 %. Figure 12 shows the Probability Density Function (PDF) for EMAC's methanol column bias when compared to IASI satellite retrievals (Franco et al., 2018) in SEA during the Indonesian peatland fires. Without VOC emissions from biomass burning, methanol is slightly underestimated by simulation REF. This underestimation is more pronounced when the in-cloud oxidation of OVOCs is taken into account (simulation $\mathrm{REF}_{\mathrm{JAMOC}}$). In both cases, EMAC tends to strongly underestimate methanol in some regions. When VOC biomass burning emissions are taken into account (simulation FIR), these underpredictions are resolved. However, now EMAC tends to strongly overestimate methanol mainly close to biomass burning sources (not shown). These overpredictions are reduced once in-cloud OVOC oxidation is implemented (simulation $\mathrm{FIR}_{\mathrm{JAMOC}}$). A high fraction of SEA is covered by oceans. Millet et al. (2008) suggested that some regions of the Pacific and Indian Ocean are a net source of methanol. As discussed by Rosanka et al. (2020b), EMAC represents the ocean as a net methanol sink. Therefore, when comparing the predictions of methanol from EMAC to satellite observations, a certain underestimation is expected. Thus, simulation $\mathrm{FIR}_{\mathrm{JAMOC}}$ compares the best with IASI retrievals, since it has overall the lowest relative biases.

Changes in hydrocarbons are minimal due to their low solubility, whereas strong changes are predicted for the relative insoluble $\mathrm{O_3}$. Due to in-cloud OVOC oxidation, the initially predicted increase in $\mathrm{O_3}$ in western Indonesia and over the Indian Ocean (Sect. 4.4) is dampened by more than 60 % once JAMOC is implemented. This reduced increase is caused by the increasing importance of clouds as $\mathrm{O_3}$ sinks. This process is globally analysed by Rosanka et al. (2020b) and is based on the enhanced $\mathrm{HO_2}$ formation in cloud droplets by OVOC oxidation. Within clouds, $\mathrm{HO_2}$ is in acid equilibrium with the superoxide anion ($\mathrm{O_2^-}$), which actively destroys $\mathrm{O_3}$.

To conclude, in-cloud OVOC oxidation is important to properly represent the resulting impacts from strong pollution events especially during the monsoon season. Overall, the predicted impact on VOCs, radicals, and $\mathrm{O_3}$ is dampened by the in-cloud oxidation and models neglecting this process probably tend to overestimate the impact of such an event. It is widely recognised that clouds may act as a source of secondary organic aerosols (SOA), which even enhances by in-cloud oxidation processes (Blando and Turpin, 2000; Ervens et al., 2011; Ervens, 2015). Ervens et al. (2011) suggested that cloud processes might contribute in the same order to SOA formation as gas-phase processes. Within this study, SOA formation from cloud processes are not explicitly represented. However, it is expected that the enhanced VOC concentrations from biomass burning will lead to an increased SOA formation from aqueous-phase processes due to the enhanced formation of oligomers (e.g. from glyoxal and methyl glyoxal) within clouds.

https://doi.org/10.5194/acp-2020-1130
Preprint. Discussion started: 17 November 2020

Atmospheric Chemistry and Physics Discussions

6 The influence of Indonesian peatland fires on the UTLS

Some of the biomass burning VOC emissions from SEA are quickly transported by the ASMA and the general tropical updraft into the UTLS (see Sect. 1 and Vogel et al., 2015), which significantly increases lower stratospheric VOC concentrations. The effect of this transport process can be observed in Fig. 11. For example, the highest increase in glyoxal, methanol, and phenol concentrations in the lower stratosphere (48.5, 33.1, and 149.4 %, respectively) is predicted in November. In the following months, these VOCs actively react with O_3 and change the lower stratospheric radical chemistry. Overall, this results in a reduction in lower stratospheric O_3 peaking in April 2016, as shown in Fig. 13. Especially in the tropics, lower stratospheric O_3 diminishes by more than 12 ppb. We find that the substantial increase in phenols, caused by the high aromatic emissions from Indonesia, favours the formation of phenoxy radicals that contribute the most to this O_3 depletion via Reaction R2. Under high-NO_x conditions, many VOCs form NO_x reservoirs (i.e. alkyl and acyl peroxy nitrates), which flattens the peak of the NO_x burden in the lower stratosphere by 7.5 % and increases the HO_2 burden by 3.3 %.

Figure 14 shows the zonal mean reduction in lower stratospheric O_3 based on the long-term simulations (simulation REF_{LONG} and FIR_{LONG}) from 2001 onward. After each Indonesian peatland fire period, stratospheric O_3 is depleted. With decreasing lower stratospheric VOC concentrations over time, O_3 slightly recovers in the second half of the following year. Particularly strong decreases are observed during El Niño periods, caused by enhanced VOC emissions from peatland fires. For example, intense fires in 2006 led to a significant decrease in lower stratospheric O_3 in early 2007. In 2010, almost no fires occurred in Indonesia (van der Werf et al., 2017), resulting in the partial recovery of lower stratospheric O_3 in 2011. Even in non El Niño years, VOC emissions from SEA biomass burning events contribute to the depletion of lower stratospheric O_3. Though of low intensity, the 2011 Indonesian peatland fires led to a reduction in O_3, which is comparable to the reduction during the 2009 El Niño year. In 2011, a strong La Niña occurred, which is the colder counterpart of El Niño (NOAA, 2020). In general, La Niña strengthens whereas El Niño weakens the ASMA. Additionally, the ASMA strengthens over time with a particular increase in 2011-2016, compared to 2001-2010 (Basha et al., 2020). Yuan et al. (2019) reported that the 2011 ASMA was stronger with a higher spatial extend. Additionally, the 2011 Indonesian fires occurred earlier during the strongest phase of the Asian monsoon. The combination of earlier fires and an enhanced updraft resultes in a higher than usual transport of VOCs to the UTLS, leading to a more important stratospheric O_3 destruction than in other non El Niño years. A higher than usual increase in UTLS CO concentrations from surface sources in 2011 was also reported by Yuan et al. (2019).

Figure 11 shows that the enhanced OVOC concentrations in the UTLS are reduced when in-cloud OVOC oxidation is taken into account. For example, EMAC predicts that the increase in the lower stratospheric methanol burden in November is reduced by about 25.5 % with the implementation of in-cloud OVOC oxidation. The increase of phenol, the aromatic that strongly contributes to the lower stratospheric O_3 destruction, is only dampened by 8.7 %. Overall, this results in a 25.2 % reduced destruction of lower stratospheric O_3 and a 19.3 % less reduction in lower stratospheric NO_x. In Fig. 3, it becomes obvious that other non-Indonesian biomass burning events occur on the Indochinese Peninsula (i.e. northwest SEA) during the Asian monsoon. VOC emissions from these fires are also transported by the ASMA into the UTLS, which contributes to the lower stratospheric O_3 depletion. Without VOC emissions from the Indonesian peatland fires (simulation FIR_{NOINDO}),

https://doi.org/10.5194/acp-2020-1130
Preprint. Discussion started: 17 November 2020

Atmospheric Chemistry and Physics Discussions

the lower stratospheric O_3 decrease is dampened by 70.3 %. This difference is almost equal to the relative contribution of Indonesia's contribution to the total SEA VOC biomass burning emissions in 2015, which accounts for 71.4 %.

In the second half of the 20th-century, stratospheric O_3 declined mainly due to halogen-containing substances from anthropogenic activities (Molina and Rowland, 1974). After the Montreal Protocol has been implemented in 1989, a slowdown of the anthropogenic stratospheric depletion was observed (Strahan and Douglass, 2018). Even though O_3 recovers in the upper- and mid-stratosphere, a decline in lower stratospheric O_3 is observed by remote sensing measurements (Kyrölä et al., 2013; Nair et al., 2015; Vigouroux et al., 2015). Recently, a lower stratospheric O_3 decline of about 1.5 DU has been reported between 2001 and 2016 by Ball et al. (2018, their Fig. 3). This reduction is mainly attributed to meteorological variability's in dynamical processes (Chipperfield et al., 2018; Ball et al., 2019). Between 2001 and 2016, we predict a lower stratospheric O_3 decrease of about 0.38 DU, when using the lower stratosphere definition of Ball et al. (2018). They define the lower stratosphere between 147-32 hPa (about 13–24 km) above 30° in latitudinal direction and between 100-32 hPa (about 17–24 km) below 30° latitude. Based on our results, we therefore appoint that biomass burning VOC emissions from SEA (in particular the Indonesian peatland fires) contribute to this observed decline by about 25 %, which is robust against the influence of in-cloud OVOC oxidation (about 20 %). To our knowledge, most global stratospheric models do not consider this kind of VOC emissions and their chemistry, and are thus not able to capture this variability. However, it is important to keep in mind that our simulations are to some degree idealised in order to be able to isolate the impact of these emissions. For example, meteorological variations induced by changes in the chemical composition are neglected.

Another interesting aspect is the reduction in lower stratospheric NO_x. In the UTLS, aviation is the only direct anthropogenic activity and contributes about 3-5 % to the total anthropogenic climate change (Lee et al., 2010). Here, aviation NO_x emissions lead to a formation of O_3 and a depletion of methane (CH_4). Recently, Rosanka et al. (2020a) showed that the enhancement in O_3 is limited by the background concentrations of NO_x and HO_x. If enough HO_x is available, a lower background NO_x concentration results in a higher O_3 gain. In general, low background HO_x concentrations limit the O_3 gain in winter. In our study, we find that in the North Atlantic flight sector (between 400–100 hPa), the NO_x burden is reduced due to SEA fires by about 6 % with regional changes of more than 20 % in 2015. At the same time, HO_x increases regionally by 10 %. Therefore, VOC emissions from frequently occurring Indonesian peatland fires potentially favour the formation of O_3 from aviation activities.

7 Model uncertainties

The most important aspects that influence our results are the representation of the transport processes, using different model resolutions, and the chemical kinetics. Each aspect is associated with some uncertainties of which all are shortly discussed in this section.

The magnitude of the depletion in lower stratospheric O_3 depends closely on the representation of the vertical transport that conveys the emitted VOCs into the UTLS. In order to evaluate the vertical transport processes of global models, ^{222}Radon (^{222}Rn, radioactive decay half-lifetime of 3.8 days) is typically used (Mahowald et al., 1997; Zhang et al., 2008; Jöckel et al.,

https://doi.org/10.5194/acp-2020-1130
Preprint. Discussion started: 17 November 2020

Atmospheric Chemistry and Physics Discussions

2010). Jöckel et al. (2010) and more recently Brinkop and Jöckel (2019) analysed the ability of EMAC to capture the $^{222}\mathrm{Rn}$ surface concentrations and vertical profiles. Their findings indicate that the vertical transport is well represented in EMAC (using the T42L90MA resolution) and that they are comparable to the earlier analysis with ECHAM5 (the base model of EMAC) by Zhang et al. (2008). Figure 4 shows that the horizontal transport is also an important aspect that influences the distribution of the emitted VOCs from Indonesian peatland fires. Evaluating the horizontal transport using observations (like $^{222}\mathrm{Rn}$) is currently not possible. Recently however, Orbe et al. (2018) compared transport time scales of various global models, including EMAC. They found that the horizontal transport from NH mid-latitudes to the tropics differs by 30 %. Based on this comparison, it can be assumed that the horizontal transport is reasonably well represented in EMAC.

In this study, we transfer our process understanding from the fine- (T106L90MA) to the coarse-resolution (T42L90MA) simulations. It is therefore important to understand how well transport processes agree between both resolutions. Currently, no direct analysis has been performed that focuses on the impact of different resolutions on transport processes in EMAC. However, Aghedo et al. (2010) analysed the influence of different horizontal and vertical resolutions in ECHAM5. Since EMAC uses the same horizontal and vertical transport scheme as ECHAM5, we assume that their findings also apply to EMAC. They find that the vertical transport mainly depends on the number of levels used. By increasing the number of layers from 19 to 31 levels, the mass transported into the stratosphere reduces globally by about 36 %, whereas increasing the resolution from T42 to T106 only decreases the vertically transported mass globally by about 10 %. Here, the influence is the lowest (about 7 %) at high latitudes and highest in the tropics (about 17 %). Aghedo et al. (2010) suggested that the higher impact in the tropics is probably related to tropical convection processes. Increasing the resolution changes the meridional transport in most regions by less than 2 % and is thus negligible. For our purposes, differences in the inter-hemispheric transport are also negligible. The mean transport time from the NH to SH decreases from 11.9 to 11.8 months and for the SH to NH transport from 11.4 to 11.5 months when increasing the horizontal resolution from T42 to T106. By using the same vertical resolution (90 levels), the highest uncertainty introduced by using different resolutions is eliminated. It is therefore expected that the important transport processes are comparable and properly represented in both resolutions.

We find that the reaction of phenoxy radicals with $\mathrm{O_3}$ (Reaction R2) has a significant influence at the surface, in the troposphere, and the lower stratosphere. As discussed by Taraborrelli et al. (2020), the chemical kinetics used in MOM to represent this $\mathrm{O_3}$ loss is associated with some uncertainties. Currently, only the measured reaction rate constant for $\mathrm{C_6H_5O}$ is available and this is used for all phenoxy radicals. Yet, no experimental evidence has been found for the formation of phenyl peroxy radical ($\mathrm{C_6H_5O_2}$), which might influence the cycling nature of this $\mathrm{O_3}$ loss by Reactions R1 and R2. However, this product is still to be expected. Even with different products, a significant deletion of $\mathrm{O_3}$ is anticipated by Reaction R2. At the same time, the reaction rate from Tao and Li (1999) is reported to be at the lower end, whereas a higher reaction rate would increase the depleted $\mathrm{O_3}$. Additionally, Taraborrelli et al. (2020) report that MOM neglects the non-HONO formation channel from nitrophenol photolysis, which does not destroy the aromatic ring and reforms phenoxy radicals (Cheng et al., 2009; Vereecken et al., 2016). It is therefore expected that, due to increasing nitrophenol concentrations in the lower troposphere (Sect. 4.5) as well as in the UTLS, the importance of Reaction R2 as an $\mathrm{O_3}$ sink is potentially underestimated.

https://doi.org/10.5194/acp-2020-1130
Preprint. Discussion started: 17 November 2020


Atmospheric Chemistry and Physics Discussions

8 Conclusions

In this study, the influence of VOC emissions from reoccurring Indonesian pealtand fires is analysed with the main focus on 2015, a particularly strong year. This is achieved by performing multiple global simulations using EMAC. By comparing EMAC's prediction of HCN columns to IASI satellite retrievals, we show that EMAC properly represents the emissions from the Indonesian peatland fires and global biomass burning events. Our results indicate that VOC emissions from biomass burning are important to reproduce hydrocarbons and secondary OVOCs in the atmosphere. Compared to other biomass burning regions, a particularly strong increase is modelled in SEA region, due to the unique emission footprint from the Indonesian peatland fires. Regionally, significant changes in radical concentrations (HO_x and NO_x) are predicted. In general, O_3 increases in the lower troposphere with the highest changes in the NH high latitudes due to strong fires in Boreal Asia. However, on a global scale, tropospheric changes in O_3 are negligible. High aromatic emissions from peatland fires lead to a depletion of O_3 in eastern Indonesia. The enhanced formation of nitrophenols and strong HNCO emissions create toxic conditions in most parts of Indonesia, directly influencing its population. The overall impact in the lower troposphere is reduced when in-cloud OVOC oxidation is taken into account. Especially, the O_3 increase initially predicted is reduced due to its enhanced destruction within clouds. However, the increased formation of oligomers in cloud droplets potentially leads to enhanced SOA concentrations.

The ongoing ASMA and the general tropical upward transport during the Indonesian fires, lift the emitted VOCs and their oxidation products quickly to the UTLS. Here, the enhanced VOC concentrations contribute to the depletion of lower stratospheric O_3. In particular, the destruction by phenoxy radicals plays a key role. The predicted O_3 depletion is in line with remote sensing measurements and supported by our results that these VOC emissions contribute by about 25 %. Although high VOC emissions from biomass burning events in ALA and NAS have a large regional impact, their impact on the UTLS is negligible due to missing fast upward transport at higher latitudes.

Appendix A: HCN retrievals from IASI observations

The spaceborne data of HCN columns used in this study are obtained from the IASI radiance spectra by applying the version 3 of the Artificial Neural Network for IASI (ANNI) retrieval framework. Initially developed for the retrieval of NH_3 and dust from the IASI observations (Whitburn et al., 2016a; Clarisse et al., 2019), ANNI v3 incorporates updates and modifications to allow the retrieval of a suite of VOCs. Until now, it has been used to retrieve methanol, formic acid, and PAN (Franco et al., 2018), then acetone (Franco et al., 2019) and acetic acid (Franco et al., 2020). Here, we perform the HCN retrieval by applying the full ANNI v3 procedure. As this approach has already been described in detail (see Franco et al., 2018, and references therein), we limit ourselves here to a summary of the main retrieval steps, and to the elements specific to the retrieval of HCN. Examples of HCN columns from IASI single overpasses in the 2015 Indonesian fire plumes and averaged distributions are also presented.

As mentioned in Sect. 2.1.3, the ANNI retrieval method proceeds in two major steps. First, in each individual IASI radiance spectrum, the target species is detected and the strength of its absorption is quantified by a metric called the Hyperspectral

https://doi.org/10.5194/acp-2020-1130
Preprint. Discussion started: 17 November 2020

Atmospheric Chemistry and Physics Discussions

Range Index (HRI). Then, the HRI is converted into a gas total column by means of an artificial feedforward neural network (NN), which also provides an uncertainty on the retrieved column.

The HRI is a dimensionless metric of the magnitude of the spectral signature of a target species in a given IASI spectrum, relative to the spectral variability of a "background" atmosphere in absence of the target gas, i.e. a variability resulting from all other parameters that contribute to the spectral radiance, such as other atmospheric gases (see Walker et al., 2011). The HRI is calculated over the main spectral range, in which the target species absorbs. The HCN absorption band (ν_2 branch) included in the IASI spectrum is situated close to a strong Q branch of CO_2 near 720 cm^{-1}. Therefore, the whole 700–800 cm^{-1} spectral range covering many HCN features is used to calculate the HRI. The CO_2 line mixing in that range is accounted for as described by Duflot et al. (2013). A first HRI of HCN was already set up for the IASI observations by Duflot et al. (2015), but here we set up a new more sensitive one following the iterative procedure presented by Franco et al. (2018).

In contrast to Duflot et al. (2015), who used pre-calculated coefficients to link the HRI to the HCN total column, the ANNI v3 procedure implements an artificial feedforward NN for this purpose. Such a NN is set up to mimic in a comprehensive way the complex connections that exist between the HRI, the state of the atmosphere and Earth's surface, and the gas abundance. Setting up a NN requires a training phase, in which the NN learns from the presentation of an extensive dataset including all the necessary input and output variables. In ANNI v3, the NN inputs are the HRI, a spectral baseline temperature, the H_2O columns, the temperature profile, the surface pressure and emissivity, and the IASI viewing angle, whereas the output is the HCN column. Here, we built this training set from over 250,000 synthetic IASI spectra simulated by a line-by-line radiative transfer model. The advantage of such a synthetic training set is that it is free of the noise and/or scarcity of real measurements and that the spectra can be generated in large amounts in order to make the training set – and hence the NN – representative of all possible conditions. For example, the NN set up for HCN is trained to retrieve gas column from 1×10^{14} to 15×10^{16} $\mathrm{molecules\,cm}^{-2}$. Actually, two separate synthetic datasets are assembled per target species, one being representative of conditions close to emission sources, the other of mixing/transport conditions (see Whitburn et al., 2016a; Franco et al., 2018, for the rationale). Each training set leads to the setup of a specific NN that is used to globally retrieve the target species in emission or transport regimes, successively. The training performances are similar to those of the other VOCs retrieved with ANNI v3 and are reached with a NN made of two computational layers, each layer deploying eight nodes.

In addition to the total column, the NN returns an associated error that is calculated via a perturbation method of the input variables (see Whitburn et al., 2016a). A pre-filter prevents the retrieval on cloudy scenes (cloud coverage > 10 %) or for observations with missing ancillary data. Consistent with the other ANNI VOCs products, a post-filter discards the individual retrievals affected by too large uncertainties or poor measurement sensitivity to HCN, specifically when

$$|\,\mathrm{column}_{(\mathrm{HCN})} \,/\, \mathrm{HRI}_{(\mathrm{HCN})}\,| \;>\; 8 \times 10^{15}\ \mathrm{molecules\,cm}^{-2} \tag{A1}$$

or spectral baseline temperatures < 268 K. This post-filter is not (directly) driven by the gas abundance, but rather by the thermal contrast (Franco et al., 2020). Finally, the constant climatological background of target gas abundance that is not accounted for by the HRI has been estimated as 1.85×10^{15} $\mathrm{molecules\,cm}^{-2}$ for HCN (see Franco et al., 2018); this offset is thus added to the individual retrieved columns. Once set up, the NN is fed for each individual IASI observation with the

https://doi.org/10.5194/acp-2020-1130
Preprint. Discussion started: 17 November 2020

Atmospheric Chemistry and Physics Discussions

appropriate input data. Here, we chose to use the ERA-5 reanalysis dataset (Hersbach et al., 2020) for the meteorological input data in the network. In the framework of the evaluation of EMAC in the 2015 Indonesian fires (see Sect. 3), only the HCN product obtained with the NN in transport/mixing regime has been exploited. Indeed, the Cloud-Aerosol Lidar with Orthogonal Polarization (CALIOP) onboard CALIPSO indicates fire plume located in the free troposphere during this massive biomass burning event.

Figure A1 presents the daily distributions of HCN total columns from IASI/Metop–A and –B observations in South-East Asia, for six successive days taken during the 2015 Indonesian fires. Whereas background areas are characterized by HCN total columns generally lower than 0.5 $\times 10^{16}$ molecules cm^{-2}, on the first day (September 29, 2015), strong HCN enhancements ($> 4 \times 10^{16}$ molecules cm^{-2}) are detected by IASI in the vicinity of Sumatra, indicating a massive fire plume. After six days (October 4, 2015), we can observe that the plume has grown progressively and that the bulk of HCN has been transported to the west across the Indian Ocean. The retrieved column uncertainties in the area generally fall in the range of 2–5$\times 10^{15}$ molecules cm^{-2}. Note that these uncertainties are reduced significantly by averaging numerous IASI measurements to build monthly or seasonal mean distributions of HCN columns. The typical seasonal distributions of IASI/Metop–A HCN columns are presented in Fig. A2 for the 2011–2014 time period, i.e. for years without massive fire events, such as the 2010 Russian fires or the 2015 Indonesian fires. These distributions highlight the dominant contribution of biomass burning to the atmospheric HCN burden, with HCN enhancements detected in Africa throughout the year, in South-East Asia in March–April–May, in India, eastern China and North Hemisphere mid- and high latitudes during the boreal summer, and within the tropics in September–October–November. Important outflows from these source regions are also noticeable, especially over the oceans. Figure A3 presents the monthly mean HCN columns during the 2015 Indonesian fires (from September to December) along with the corresponding distributions over the 2011–2014 time period. It illustrates the exceptional intensity of the 2015 fires compared to the previous years, with important HCN enhancements detected throughout the entire intertropical band.

Data availability. The simulation results are archived at the Jülich Supercomputing Centre (JSC) and are available on request. The IASI VOC columns retrieved with the ANNI framework are available upon request.

Author contributions. The study was designed by SR and DT. SR performed the simulations and analysed the data with contributions from DT. BF, LC, and PFC developed the IASI products and acted as analysts. SR and DT discussed the results with contributions from BF and AW. The manuscript was prepared by SR with the help of all co-authors.

Competing interests. The authors declare that they have no competing of interest.

https://doi.org/10.5194/acp-2020-1130
Preprint. Discussion started: 17 November 2020

Atmospheric Chemistry and Physics Discussions

Acknowledgements. The work described in this paper has received funding from the Initiative and Networking Fund of the Helmholtz Association through the project "Advanced Earth System Modelling Capacity (ESM)". The content of this paper is the sole responsibility of the author(s) and it does not represent the opinion of the Helmholtz Association, and the Helmholtz Association is not responsible for any use that might be made of the information contained. The authors gratefully acknowledge the Earth System Modelling Project (ESM) for funding this work by providing computing time on the ESM partition of the supercomputer JUWELS at the Jülich Supercomputing Centre (JSC). IASI is a joint mission of EUMETSAT and the Centre National d'Etudes Spatiales (CNES, France). The research at ULB has been supported by the project OCTAVE (Oxygenated Compounds in the Tropical Atmosphere: Variability and Exchanges (http://octave.aeronomie.be/) of the Belgian Research Action through Interdisciplinary Networks (BRAIN-be; 2017–2021; Research project BR/175/A2/OCTAVE) and by the IASI.Flow Prodex arrangement (ESA–BELSPO). LC is a research associate supported by the F.R.S.–FNRS.

https://doi.org/10.5194/acp-2020-1130
Preprint. Discussion started: 17 November 2020

Atmospheric Chemistry and Physics Discussions

Table 1. Characteristics of the different biomass burning regions focusing on the dominant fire type, the main biomass burning season, and the Dry Matter Burned (DMB). The global DMB in 2015 is 4985 $\mathrm{Tg\,a^{-1}}$. The naming of each region is as follows: ALA = Alaska, CAF = Central Africa, CSA = Central South America, NAS = North Asia, NAU = North Australia, SAF = South Africa, and SEA = South East Asia. Each region is graphically illustrated in Fig. 2.

Region	Dominant fire type	Main biomass burning season	2015 DMB [$\mathrm{Tg\,a^{-1}}$]
ALA	Extratropical forest with organic soil	JJA	295
CAF	Tropical forest & Savanna	DJF	778
CSA	Savanna	SON	439
NAS	Extratropical forest with organic soil	MMA & JJA	363
NAU	Savanna	SON	260
SAF	Tropical forest & Savanna	JJA	1036
SEA	Tropical forest[a]	SON	1237[b]

[a]In this study a combination of tropical forest (50 %) & peatland (50 %) is assumed in Indonesia (Sect. 2.1.2)
[b]Of which 949 $\mathrm{Tg\,a^{-1}}$ are from Indonesian peatland fires

Table 2. List of EMAC simulations performed in this study.

Name	Analysed Period	VOC Bioburn Emissions	Aqueous-phase mechanism	Resolution
REF	2015-2016	no	ScSta	T106L90MA
FIR	2015-2016	yes	ScSta	T106L90MA
$\mathrm{FIR_{NOINDO}}$	SOND[a] in 2015	yes[b]	ScSta	T106L90MA
$\mathrm{REF_{LONG}}$	2001-2016	no	ScSta	T42L90MA
$\mathrm{FIR_{LONG}}$	2001-2016	yes	ScSta	T42L90MA
$\mathrm{REF_{JAMOC}}$	SOND[a] in 2015	no	JAMOC	T106L90MA
$\mathrm{FIR_{JAMOC}}$	SOND[a] in 2015	yes	JAMOC	T106L90MA

[a]Focus on Indonesia in September, October, November, and December
[b]No VOC biomass burning emissions from Indonesian peatland fires

https://doi.org/10.5194/acp-2020-1130
Preprint. Discussion started: 17 November 2020

Atmospheric Chemistry and Physics Discussions

Table 3. Absolute changes in the tropospheric burden for each region and each species discussed. Regional differences are calculated for the main biomass burning season (see Table 1) and the global changes are calculated for the complete year of 2015. If not stated otherwise, absolute differences are given in Gg and relative changes are provided in parenthesis in %. Most radical burdens are presented in mol. The differences are calculated between simulation REF and FIR.

Species	Global		ALA		CAF		CSA		NAS		NAU		SAF		SEA	
Hydrocarbons																
Acetylene	45.7	(20.5)	1.4	(119.8)	4.4	(56.0)	6.0	(305.0)	2.5	(20.8)	2.8	(258.8)	6.6	(184.5)	13.2	(64.2)
Ethane	422.9	(32.6)	20.4	(140.1)	18.4	(43.6)	23.9	(144.9)	31.8	(47.3)	16.7	(128.3)	26.5	(123.8)	47.6	(48.2)
Aromatics																
Benzene	38.8	(27.3)	4.4	(1312.7)	2.7	(46.4)	4.3	(368.2)	5.9	(84.2)	1.9	(498.1)	4.6	(228.7)	20.0	(207.7)
Toluene	6.7	(15.3)	0.8	(1308.7)	0.6	(62.8)	1.0	(85.0)	1.0	(62.0)	0.2	(198.2)	0.9	(199.0)	10.2	(366.8)
Phenol	1.1	(105.7)	0.2	(4282.2)	0.2	(316.4)	0.3	(1305.1)	0.1	(323.5)	0.1	(1353.8)	0.3	(1339.7)	1.3	(1226.3)
OVOCs																
Methanol	223.3	(7.9)	11.7	(31.6)	17.0	(16.8)	31.5	(6.6)	18.8	(16.2)	14.4	(17.5)	27.4	(28.5)	112.3	(60.7)
Glyoxal	3.9	(9.3)	0.4	(126.2)	0.6	(24.5)	0.6	(3.9)	0.4	(38.6)	0.2	(12.7)	1.0	(36.7)	3.2	(62.2)
Methyl glyoxal	2.5	(1.3)	0.2	(17.4)	0.4	(4.1)	0.2	(0.2)	0.2	(6.9)	0.1	(1.3)	0.7	(5.8)	2.2	(10.2)
CO	8341.1	(2.4)	153.3	(3.9)	253.4	(2.4)	446.4	(2.8)	307.5	(2.6)	503.2	(6.2)	273.4	(3.4)	1908.0	(6.5)
Acids																
Formic acid	32.9	(4.9)	1.5	(24.0)	7.0	(25.2)	5.8	(4.7)	2.1	(12.9)	3.2	(13.0)	11.4	(49.9)	11.3	(20.7)
Acetic acid	119.3	(23.3)	8.7	(441.7)	29.0	(124.3)	34.1	(15.3)	9.8	(128.5)	10.4	(45.3)	48.7	(238.9)	37.7	(117.4)
Oxidants																
O_3	1115.3	(0.3)	92.0	(1.9)	61.6	(0.7)	-28.3	(-0.3)	104.7	(0.7)	2.0	(0.0)	60.4	(0.8)	83.2	(0.4)
OH [$\times 10^3$ mol]	-240.3	(-1.7)	-6.4	(-4.9)	-8.5	(-2.4)	-15.9	(-4.7)	-10.8	(-3.4)	-21.6	(-6.8)	-10.3	(-3.5)	-58.2	(-4.5)
HO_2 [$\times 10^4$ mol]	353.7	(0.4)	35.5	(3.7)	41.0	(1.7)	36.8	(0.8)	41.0	(1.8)	15.8	(0.7)	53.3	(2.8)	94.5	(1.3)
NO [$\times 10^6$ mol]	-82.3	(-2.8)	-38.4	(-52.7)	-5.9	(-6.5)	-5.7	(-6.6)	-26.0	(-26.6)	-6.8	(-10.6)	-6.4	(-7.5)	-22.0	(-7.7)
NO_2 [$\times 10^6$ mol]	-178.5	(-2.2)	-73.5	(-36.7)	-16.3	(-4.7)	-14.2	(-4.1)	-60.1	(-19.3)	-13.0	(-6.5)	-18.8	(-5.5)	-70.5	(-8.3)
NO_3 [$\times 10^6$ mol]	6.9	(5.3)	0.2	(35.5)	0.4	(6.0)	0.2	(6.6)	0.4	(15.2)	0.5	(16.9)	0.4	(9.3)	2.4	(15.5)

https://doi.org/10.5194/acp-2020-1130
Preprint. Discussion started: 17 November 2020

Atmospheric Chemistry and Physics Discussions

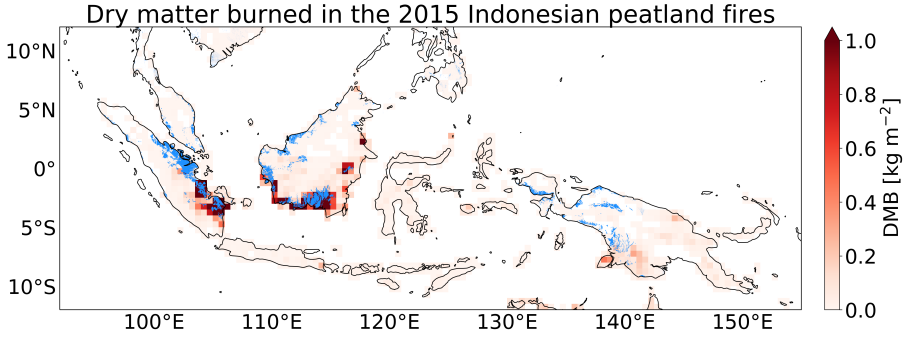

Figure 1. Accumulated dry matter burned (DMB) during the Indonesian peatland fires of 2015. The distribution of Indonesian peatland is indicated in blue. The data for the peatland distribution are obtained from Xu et al. (2017, 2018).

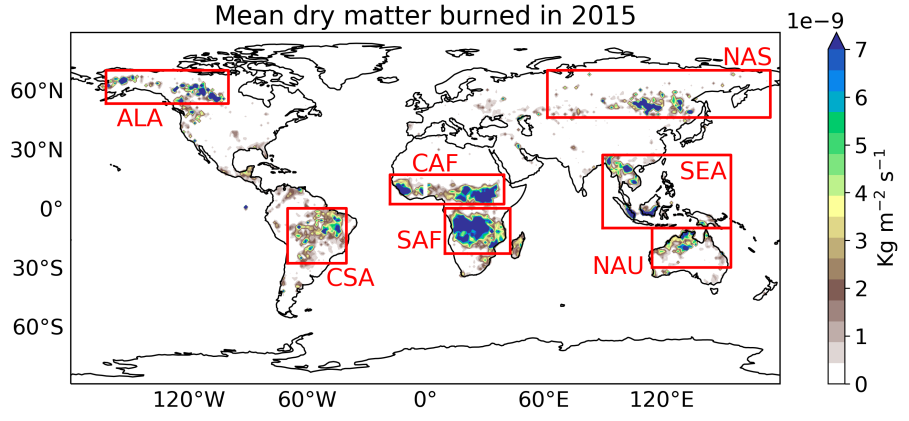

Figure 2. Mean dry matter burned (DMB) in 2015. The naming of each region is as follows: ALA = Alaska, CAF = Central Africa, CSA = Central South America, NAS = North Asia, NAU = North Australia, SAF = South Africa, and SEA = South East Asia. Further details about each region are presented in Table 1.

https://doi.org/10.5194/acp-2020-1130
Preprint. Discussion started: 17 November 2020

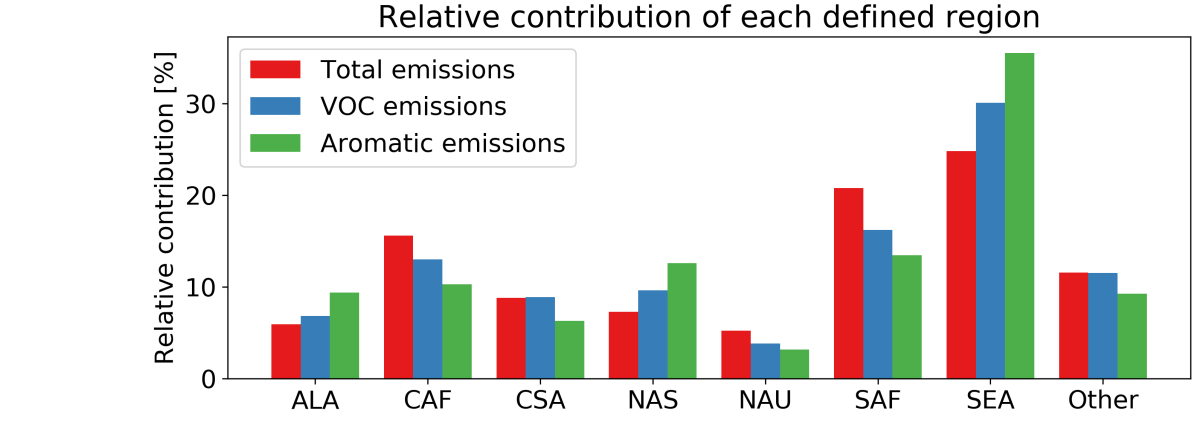

Figure 3. Relative contribution of each defined emission region to the total, the VOC, and the aromatic emissions from biomass burning in 2015. Further details about each region are presented in Table 1 and Fig. 2.

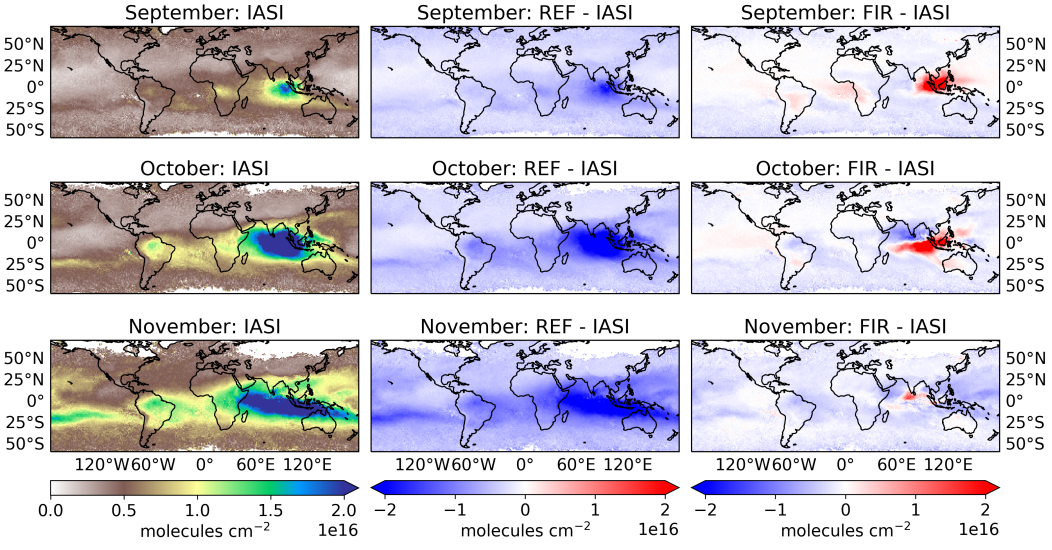

Figure 4. HCN column comparison between IASI satellite observations and EMAC for September, October and November 2015. IASI satellite observations (left), the simulation without VOC biomass burning emissions (simulation REF) in comparison to IASI observations (centre), and the simulation including VOC biomass burning emissions (simulation FIR) in comparison to IASI observations (right).

https://doi.org/10.5194/acp-2020-1130
Preprint. Discussion started: 17 November 2020

Atmospheric Chemistry and Physics Discussions

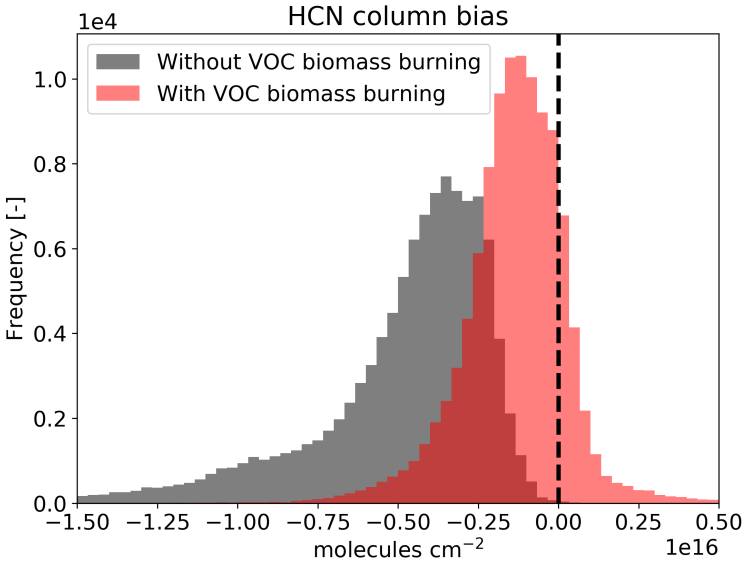

Figure 5. Global HCN column bias between EMAC simulations and IASI satellite data. The column bias is calculated based on monthly mean data during the Indonesian peatland fires in 2015.

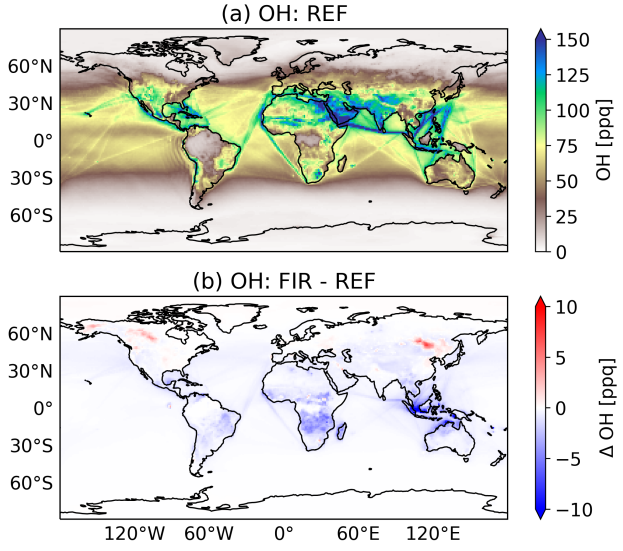

Figure 6. (a) Yearly mean surface OH concentration without biomass burning VOC emissions. (b) Changes in the yearly mean surface OH concentration due to VOC biomass burning.

https://doi.org/10.5194/acp-2020-1130
Preprint. Discussion started: 17 November 2020

Atmospheric Chemistry and Physics Discussions

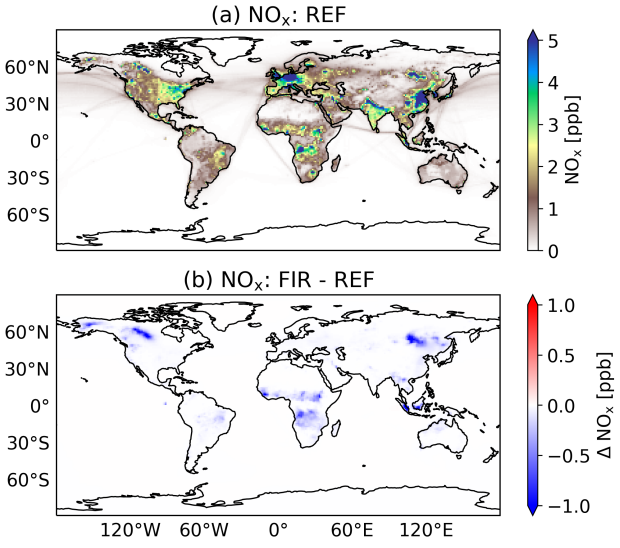

Figure 7. (a) Yearly mean surface NO_x concentration without biomass burning VOC emissions. (b) Changes in the yearly mean surface NO_x concentration due to VOC biomass burning.

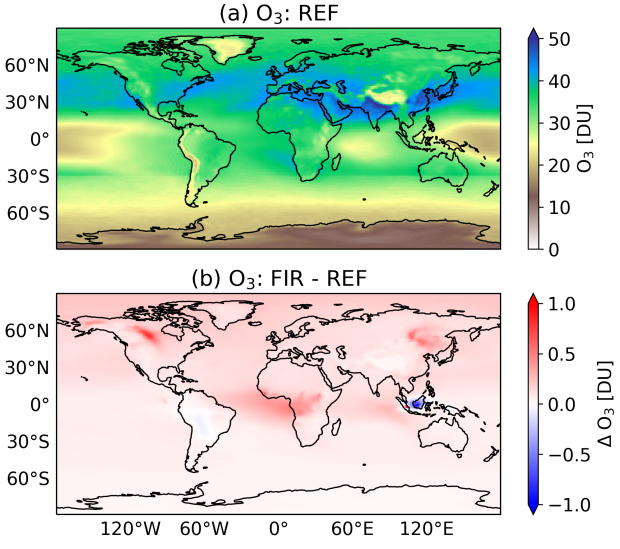

Figure 8. (a) Yearly mean tropospheric O_3 column without biomass burning VOC emissions. (b) Changes in the yearly mean tropospheric O_3 column due to VOC biomass burning.

https://doi.org/10.5194/acp-2020-1130
Preprint. Discussion started: 17 November 2020

Atmospheric Chemistry and Physics Discussions

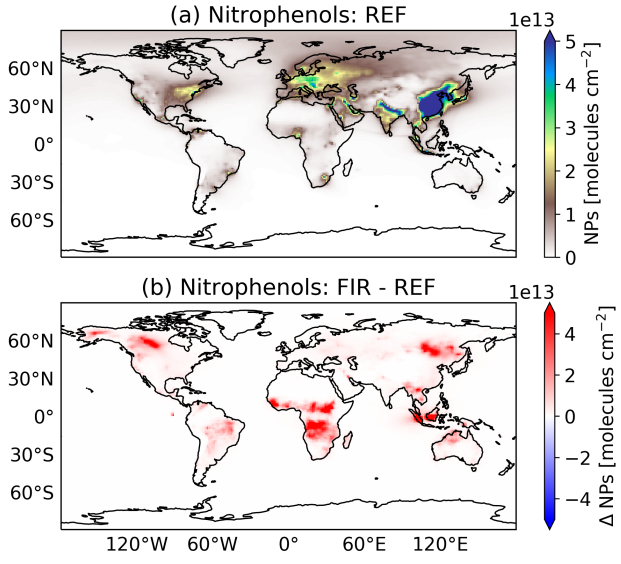

Figure 9. (a) Yearly mean tropospheric nitrophenol (NPs) column without biomass burning VOC emissions. (b) Changes in the yearly mean tropospheric nitrophenol (NPs) due to VOC biomass burning.

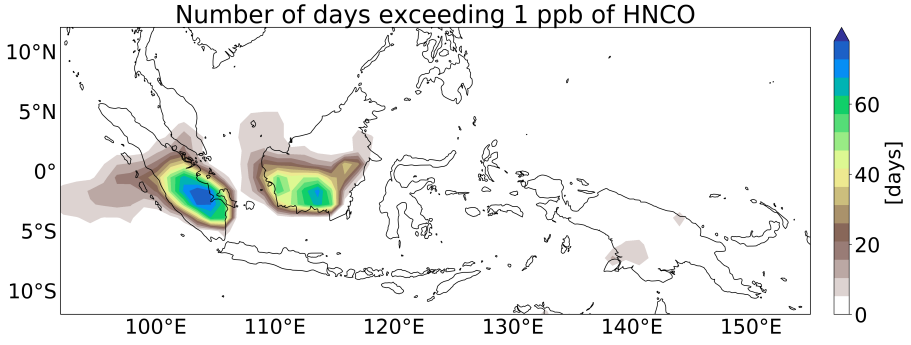

Figure 10. Number of days in which ambient concentrations of 1 ppb of HNCO are exceeded during the Indonesian peatland fires in 2015.

https://doi.org/10.5194/acp-2020-1130
Preprint. Discussion started: 17 November 2020

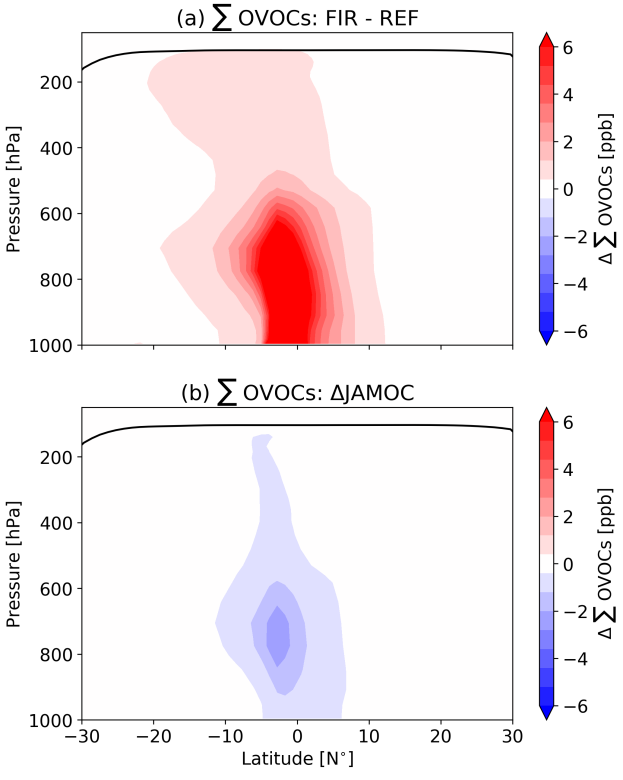

Figure 11. Mean zonal change in the sum of all OVOCs explicitly reacting in JAMOC over Indonesia and the Indian Ocean during the 2015 Indonesian fire period (SON). (a) Changes due to VOC biomass burning emissions (difference between simulation FIR and REF) and (b) changes due to JAMOC (ΔJAMOC).

https://doi.org/10.5194/acp-2020-1130
Preprint. Discussion started: 17 November 2020

Atmospheric Chemistry and Physics Discussions

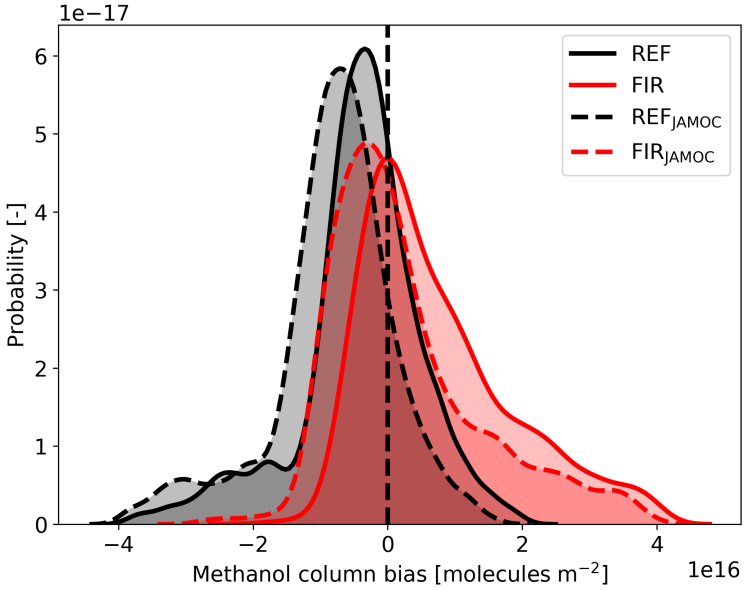

Figure 12. Probability density function of EMAC's methanol column bias to the IASI satellite measurements for simulation REF, FIR, $\mathrm{REF_{JAMOC}}$, and $\mathrm{FIR_{JAMOC}}$ in SEA during the 2015 Indonesian peatland fires.

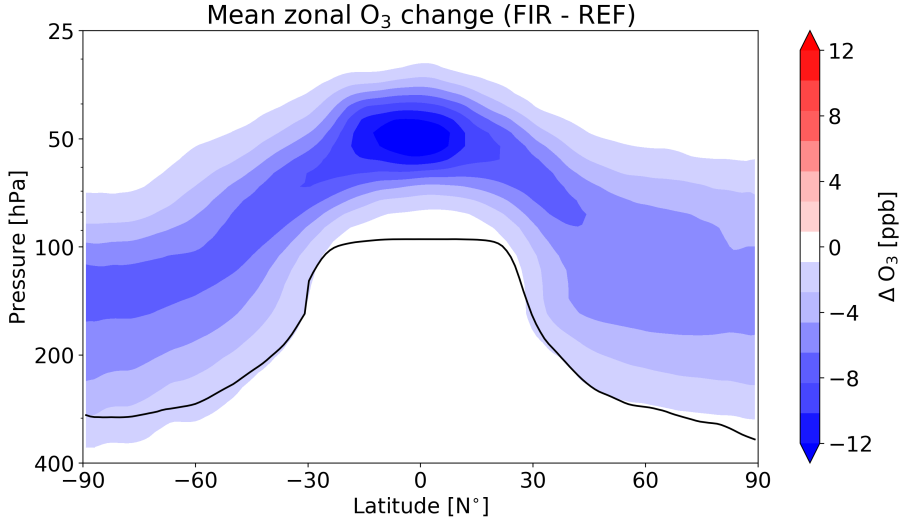

Figure 13. Mean zonal O_3 change in the UTLS in April 2016. The difference is calculated based on simulation FIR and REF. The tropopause is depicted by the black line.

https://doi.org/10.5194/acp-2020-1130
Preprint. Discussion started: 17 November 2020

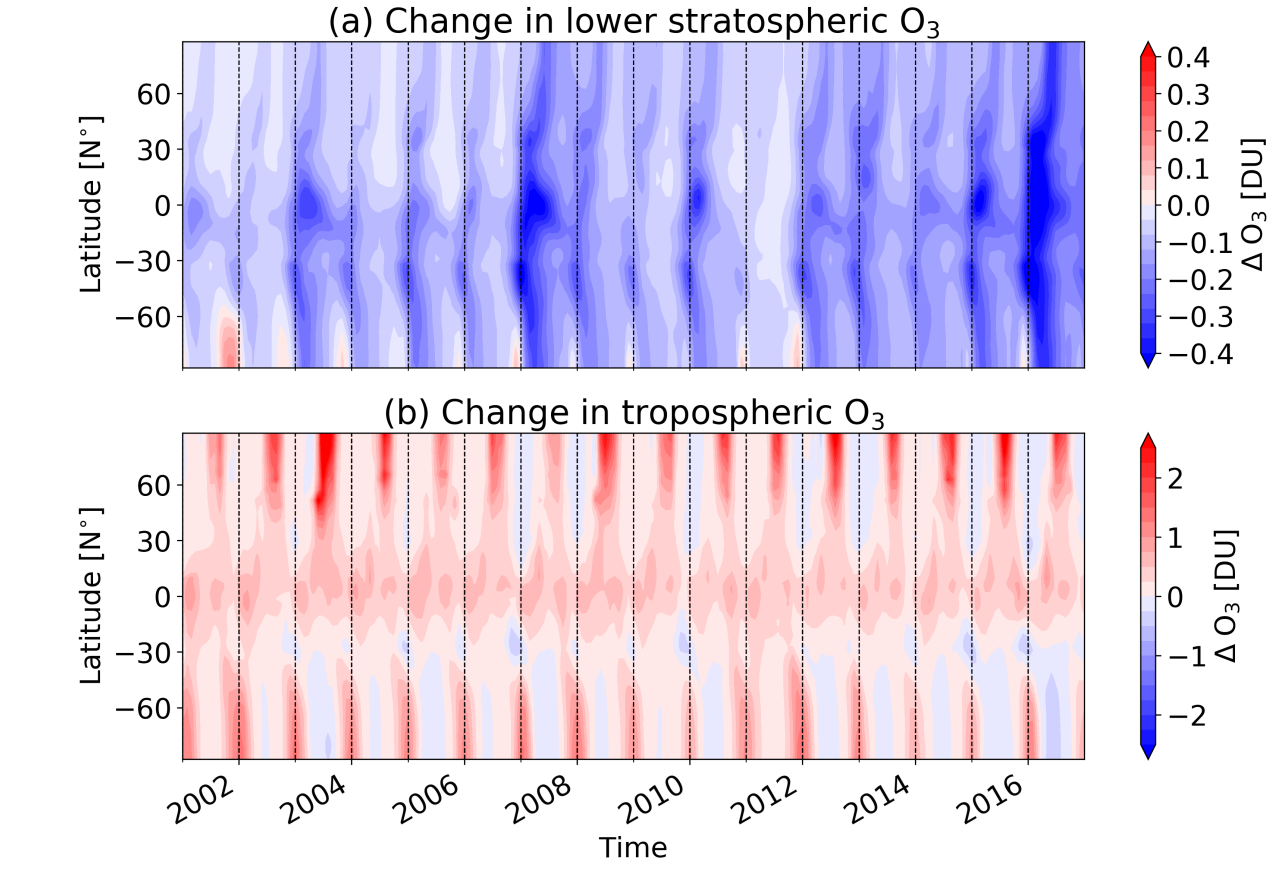

Figure 14. Zonal mean change in column O_3 between simulation FIR and REF for (a) the lower stratosphere defined from the tropopause to 32 hPa and (b) the troposphere defined from the surface to the tropopause. The tropopause is defined using EMAC's standard definition, which defines the tropopause in the extra tropics using potential vorticity and temperature lapse rates in the tropics (following Jöckel et al., 2006).

https://doi.org/10.5194/acp-2020-1130
Preprint. Discussion started: 17 November 2020

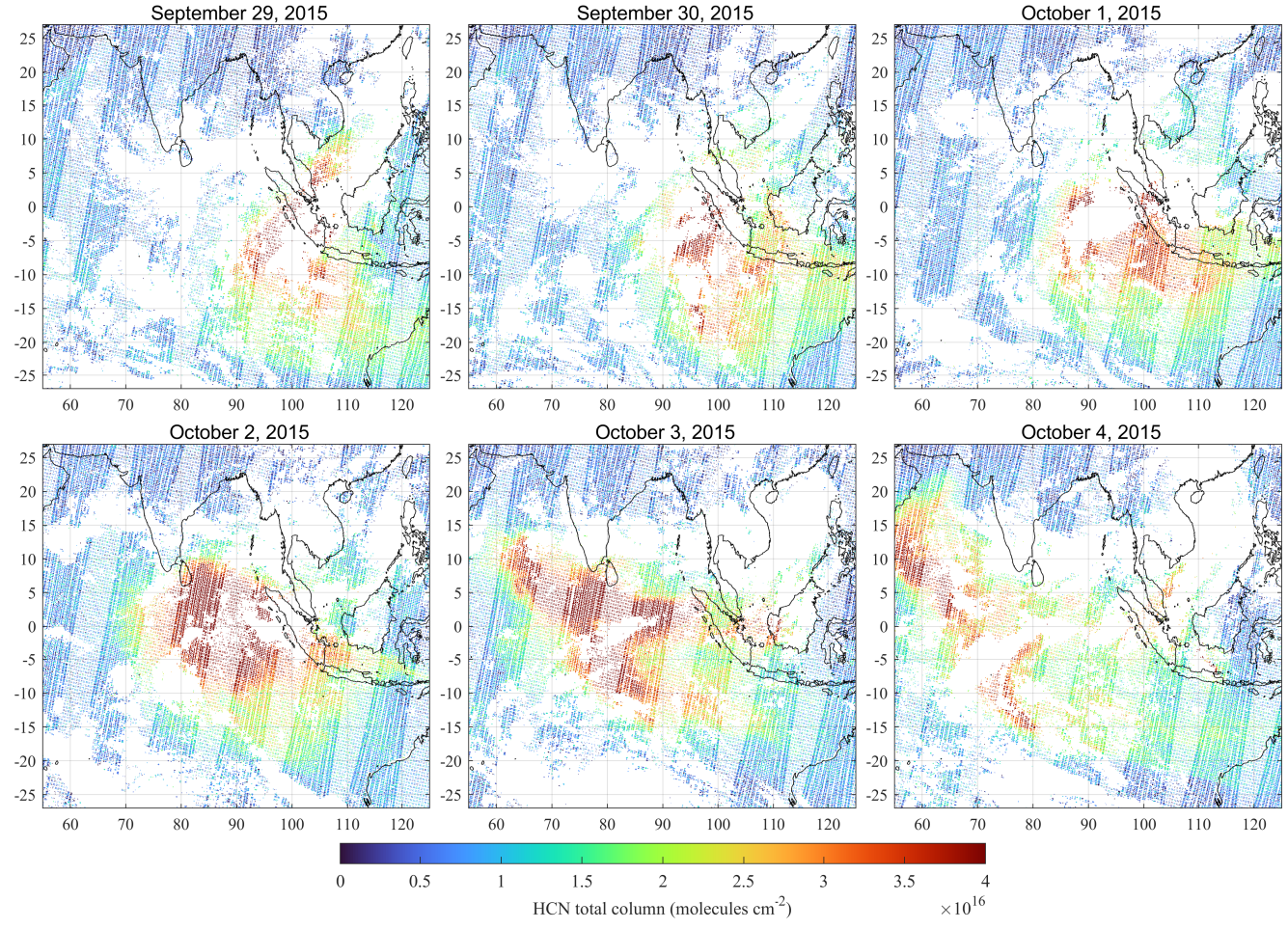

Figure A1. Daily regional distributions of HCN total column (in molecules cm^{-2}) derived from the IASI spectra recorded in the morning overpasses of Metop–A and –B, for six successive days during the 2015 Indonesian fires. These distributions take into account the actual footprint on the Earth's surface of each individual IASI measurement, i.e. a small circle at nadir and an elongated ellipse at the limit of the across-track swath of the satellite. Note the complementarity of the IASI/Metop–A and –B flight tracks that avoid gaps between the successive overpasses in the tropics. The white areas correspond to data filtered out because of unsatisfactory retrieval quality or the presence of clouds.

https://doi.org/10.5194/acp-2020-1130
Preprint. Discussion started: 17 November 2020

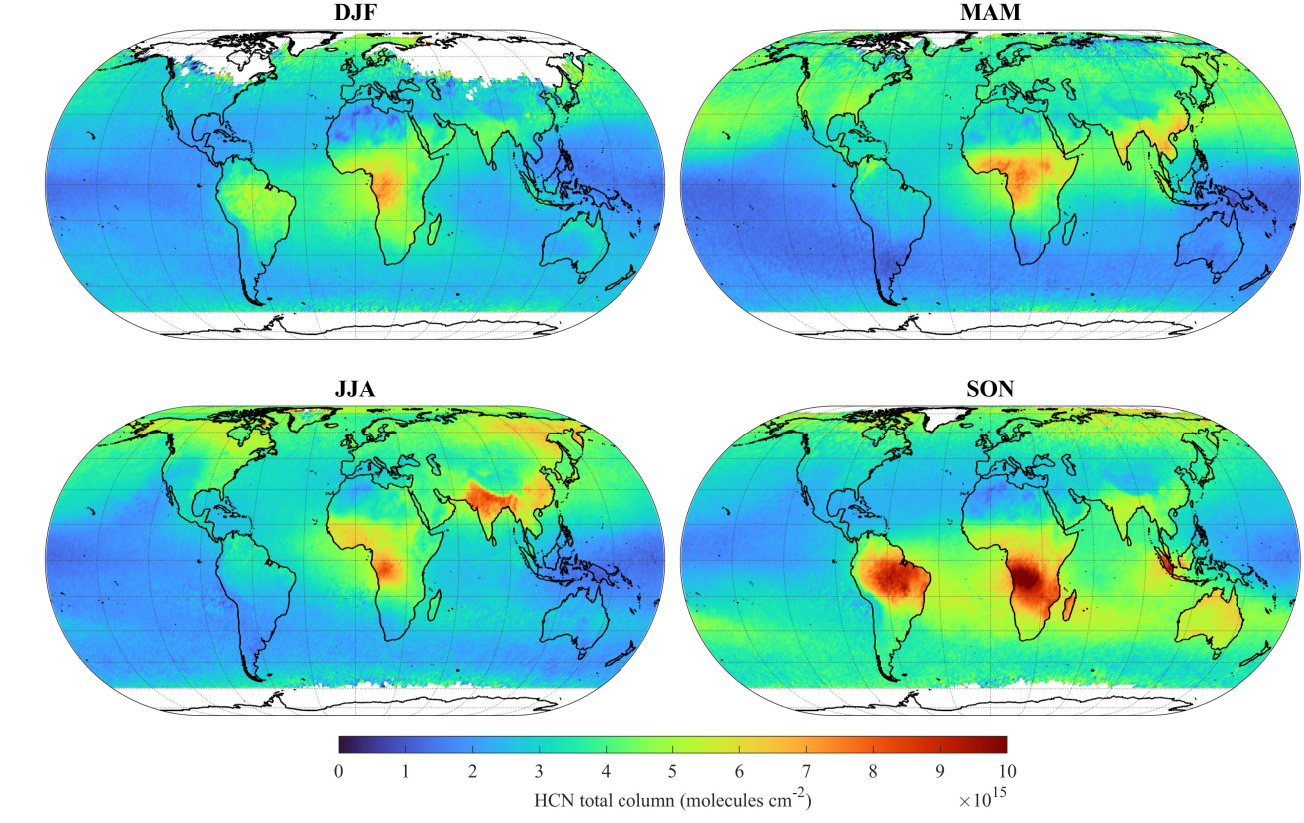

Figure A2. Seasonal means (on a 1 × 1° grid) of the HCN total columns (in molecules cm^{-2}) retrieved from the IASI/Metop–A measurements over the 2011–2014 time period. The HCN columns over the continents have been retrieved with the NN in emission regime, whereas the NN in transport/mixing regime has been used over the oceans.

https://doi.org/10.5194/acp-2020-1130
Preprint. Discussion started: 17 November 2020

Atmospheric Chemistry and Physics Discussions

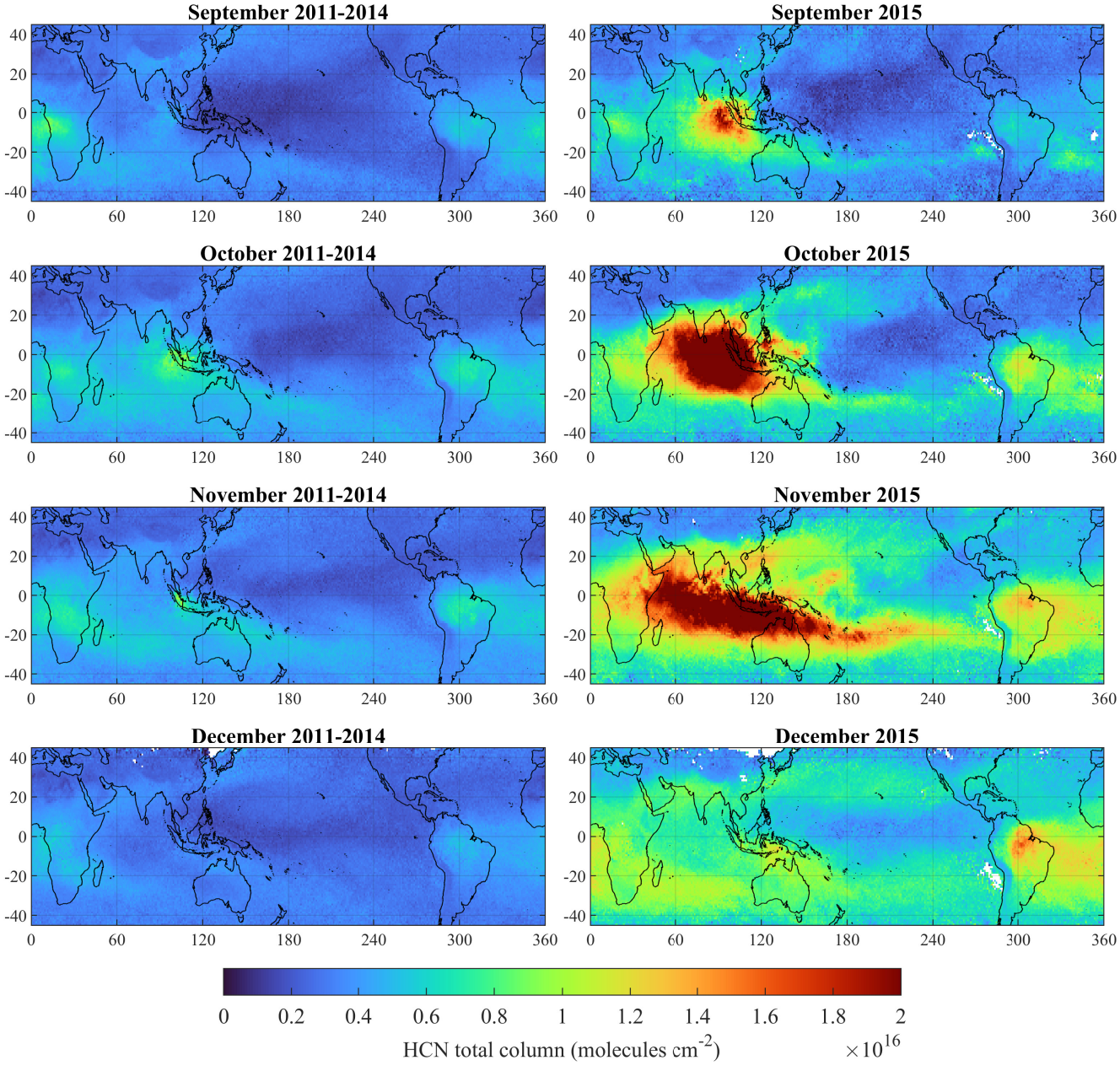

Figure A3. Monthly means (on a 1 × 1° grid) of the HCN total columns (in molecules cm^{-2}) retrieved from the IASI/Metop–A measurements over the 2011–2014 time period (left plots) and over the year 2015 (right plots).

https://doi.org/10.5194/acp-2020-1130
Preprint. Discussion started: 17 November 2020

References

Aghedo, A. M., Rast, S., and Schultz, M. G.: Sensitivity of tracer transport to model resolution, prescribed meteorology and tracer lifetime in the general circulation model ECHAM5, Atmospheric Chemistry and Physics, 10, 3385–3396, https://doi.org/10.5194/acp-10-3385-2010, 2010.

Akagi, S. K., Yokelson, R. J., Wiedinmyer, C., Alvarado, M. J., Reid, J. S., Karl, T., Crounse, J. D., and Wennberg, P. O.: Emission factors for open and domestic biomass burning for use in atmospheric models, Atmospheric Chemistry and Physics, 11, 4039–4072, https://doi.org/10.5194/acp-11-4039-2011, 2011.

Andreae, M. O.: Emission of trace gases and aerosols from biomass burning – an updated assessment, Atmospheric Chemistry and Physics, 19, 8523–8546, https://doi.org/10.5194/acp-19-8523-2019, 2019.

Atkinson, R., Carter, W. P. L., Darnall, K. R., Winer, A. M., and Pitts Jr., J. N.: A smog chamber and modeling study of the gas phase NOx–air photooxidation of toluene and the cresols, International Journal of Chemical Kinetics, 12, 779–836, https://doi.org/10.1002/kin.550121102, 1980.

Ball, W. T., Alsing, J., Mortlock, D. J., Staehelin, J., Haigh, J. D., Peter, T., Tummon, F., Stübi, R., Stenke, A., Anderson, J., Bourassa, A., Davis, S. M., Degenstein, D., Frith, S., Froidevaux, L., Roth, C., Sofieva, V., Wang, R., Wild, J., Yu, P., Ziemke, J. R., and Rozanov, E. V.: Evidence for a continuous decline in lower stratospheric ozone offsetting ozone layer recovery, Atmospheric Chemistry and Physics, 18, 1379–1394, https://doi.org/10.5194/acp-18-1379-2018, 2018.

Ball, W. T., Alsing, J., Staehelin, J., Davis, S. M., Froidevaux, L., and Peter, T.: Stratospheric ozone trends for 1985–2018: sensitivity to recent large variability, Atmospheric Chemistry and Physics, 19, 12 731–12 748, https://doi.org/10.5194/acp-19-12731-2019, 2019.

Basha, G., Ratnam, M. V., and Kishore, P.: Asian summer monsoon anticyclone: trends and variability, Atmospheric Chemistry and Physics, 20, 6789–6801, https://doi.org/10.5194/acp-20-6789-2020, 2020.

Blando, J. D. and Turpin, B. J.: Secondary organic aerosol formation in cloud and fog droplets: a literature evaluation of plausibility, Atmospheric Environment, 34, 1623 – 1632, https://doi.org/10.1016/S1352-2310(99)00392-1, 2000.

Brinkop, S. and Jöckel, P.: ATTILA 4.0: Lagrangian advective and convective transport of passive tracers within the ECHAM5/MESSy (2.53.0) chemistry–climate model, Geoscientific Model Development, 12, 1991–2008, https://doi.org/10.5194/gmd-12-1991-2019, 2019.

Cabrera-Perez, D., Taraborrelli, D., Sander, R., and Pozzer, A.: Global atmospheric budget of simple monocyclic aromatic compounds, Atmospheric Chemistry and Physics, 16, 6931–6947, https://doi.org/10.5194/acp-16-6931-2016, 2016.

Cheng, S.-B., Zhou, C.-H., Yin, H.-M., Sun, J.-L., and Han, K.-L.: OH produced from o-nitrophenol photolysis: A combined experimental and theoretical investigation, The Journal of Chemical Physics, 130, 234 311, https://doi.org/10.1063/1.3152635, 2009.

Chipperfield, M. P., Dhomse, S., Hossaini, R., Feng, W., Santee, M. L., Weber, M., Burrows, J. P., Wild, J. D., Loyola, D., and Coldewey-Egbers, M.: On the Cause of Recent Variations in Lower Stratospheric Ozone, Geophysical Research Letters, 45, 5718–5726, https://doi.org/10.1029/2018GL078071, 2018.

Christian, T. J., Kleiss, B., Yokelson, R. J., Holzinger, R., Crutzen, P. J., Hao, W. M., Saharjo, B. H., and Ward, D. E.: Comprehensive laboratory measurements of biomass-burning emissions: 1. Emissions from Indonesian, African, and other fuels, Journal of Geophysical Research: Atmospheres, 108, https://doi.org/10.1029/2003JD003704, 2003.

Cicerone, R. J. and Zellner, R.: The atmospheric chemistry of hydrogen cyanide (HCN), Journal of Geophysical Research: Oceans, 88, 10 689–10 696, https://doi.org/10.1029/JC088iC15p10689, 1983.

https://doi.org/10.5194/acp-2020-1130
Preprint. Discussion started: 17 November 2020

Clarisse, L., Clerbaux, C., Franco, B., Hadji-Lazaro, J., Whitburn, S., Kopp, A. K., Hurtmans, D., and Coheur, P.-F.: A Decadal Data Set of Global Atmospheric Dust Retrieved From IASI Satellite Measurements, Journal of Geophysical Research: Atmospheres, 124, 1618–1647, https://doi.org/10.1029/2018jd029701, 2019.

Clerbaux, C., Boynard, A., Clarisse, L., George, M., Hadji-Lazaro, J., Herbin, H., Hurtmans, D., Pommier, M., Razavi, A., Turquety, S., Wespes, C., and Coheur, P.-F.: Monitoring of atmospheric composition using the thermal infrared IASI/MetOp sounder, Atmospheric Chemistry and Physics, 9, 6041–6054, https://doi.org/10.5194/acp-9-6041-2009, 2009.

Crippa, P., Castruccio, S., Archer-Nicholls, S., Lebron, G. B., Kuwata, M., Thota, A., Sumin, S., Butt, E., Wiedinmyer, C., and Spracklen, D. V.: Population exposure to hazardous air quality due to the 2015 fires in Equatorial Asia, Scientific Reports, 6, 37 074, https://doi.org/10.1038/srep37074, 2016.

Duflot, V., Hurtmans, D., Clarisse, L., R'honi, Y., Vigouroux, C., Mazière, M. D., Mahieu, E., Servais, C., Clerbaux, C., and Coheur, P.-F.: Measurements of hydrogen cyanide (HCN) and acetylene (C2H2) from the Infrared Atmospheric Sounding Interferometer (IASI), Atmospheric Measurement Techniques, 6, 917–925, https://doi.org/10.5194/amt-6-917-2013, 2013.

Duflot, V., Wespes, C., Clarisse, L., Hurtmans, D., Ngadi, Y., Jones, N., Paton-Walsh, C., Hadji-Lazaro, J., Vigouroux, C., Mazière, M. D., Metzger, J.-M., Mahieu, E., Servais, C., Hase, F., Schneider, M., Clerbaux, C., and Coheur, P.-F.: Acetylene (C2H2) and hydrogen cyanide (HCN) from IASI satellite observations: global distributions, validation, and comparison with model, Atmospheric Chemistry and Physics, 15, 10 509–10 527, https://doi.org/10.5194/acp-15-10509-2015, 2015.

Ervens, B.: Modeling the Processing of Aerosol and Trace Gases in Clouds and Fogs, Chemical Reviews, 115, 4157–4198, https://doi.org/10.1021/cr5005887, 2015.

Ervens, B., Turpin, B. J., and Weber, R. J.: Secondary organic aerosol formation in cloud droplets and aqueous particles (aqSOA): a review of laboratory, field and model studies, Atmospheric Chemistry and Physics, 11, 11 069–11 102, https://doi.org/10.5194/acp-11-11069-2011, 2011.

Franco, B., Clarisse, L., Stavrakou, T., Müller, J.-F., Van Damme, M., Whitburn, S., Hadji-Lazaro, J., Hurtmans, D., Taraborrelli, D., Clerbaux, C., and Coheur, P.-F.: A General Framework for Global Retrievals of Trace Gases From IASI: Application to Methanol, Formic Acid, and PAN, Journal of Geophysical Research: Atmospheres, 123, 13,963–13,984, https://doi.org/10.1029/2018JD029633, 2018.

Franco, B., Clarisse, L., Stavrakou, T., Müller, J.-F., Pozzer, A., Hadji-Lazaro, J., Hurtmans, D., Clerbaux, C., and Coheur, P.-F.: Acetone Atmospheric Distribution Retrieved From Space, Geophysical Research Letters, 46, 2884–2893, https://doi.org/10.1029/2019gl082052, 2019.

Franco, B., Clarisse, L., Stavrakou, T., Müller, J.-F., Taraborrelli, D., Hadji-Lazaro, J., Hannigan, J. W., Hase, F., Hurtmans, D., Jones, N., Lutsch, E., Mahieu, E., Ortega, I., Schneider, M., Strong, K., Vigouroux, C., Clerbaux, C., and Coheur, P.-F.: Space-borne Measurements of Formic and Acetic Acids: A Global View of the Regional Sources, Geophysical Research Letters, 47, https://doi.org/10.1029/2019gl086239, 2020.

Fu, R., Hu, Y., Wright, J. S., Jiang, J. H., Dickinson, R. E., Chen, M., Filipiak, M., Read, W. G., Waters, J. W., and Wu, D. L.: Short circuit of water vapor and polluted air to the global stratosphere by convective transport over the Tibetan Plateau, Proceedings of the National Academy of Sciences, 103, 5664–5669, https://doi.org/10.1073/pnas.0601584103, 2006.

Gaveau, D. L. A., Salim, M. A., Hergoualc'h, K., Locatelli, B., Sloan, S., Wooster, M., Marlier, M. E., Molidena, E., Yaen, H., DeFries, R., Verchot, L., Murdiyarso, D., Nasi, R., Holmgren, P., and Sheil, D.: Major atmospheric emissions from peat fires in Southeast Asia during non-drought years: evidence from the 2013 Sumatran fires, Scientific Reports, 4, 6112, https://doi.org/10.1038/srep06112, 2014.

https://doi.org/10.5194/acp-2020-1130
Preprint. Discussion started: 17 November 2020

Grosjean, D.: Atmospheric reactions of ortho cresol: Gas phase and aerosol products, Atmospheric Environment (1967), 18, 1641 – 1652, https://doi.org/10.1016/0004-6981(84)90386-X, 1984.

Grosjean, D.: Atmospheric fate of toxic aromatic compounds, Science of The Total Environment, 100, 367 – 414, https://doi.org/10.1016/0048-9697(91)90386-S, an Honour Volume For Eric I. Hamilton, 1991.

Guenther, A., Karl, T., Harley, P., Wiedinmyer, C., Palmer, P. I., and Geron, C.: Estimates of global terrestrial isoprene emissions using MEGAN (Model of Emissions of Gases and Aerosols from Nature), Atmospheric Chemistry and Physics, 6, 3181–3210, https://doi.org/10.5194/acp-6-3181-2006, 2006.

Hems, R. F. and Abbatt, J. P. D.: Aqueous Phase Photo-oxidation of Brown Carbon Nitrophenols: Reaction Kinetics, Mechanism, and Evolution of Light Absorption, ACS Earth and Space Chemistry, 2, 225–234, https://doi.org/10.1021/acsearthspacechem.7b00123, 2018.

Hens, K., Novelli, A., Martinez, M., Auld, J., Axinte, R., Bohn, B., Fischer, H., Keronen, P., Kubistin, D., Nölscher, A. C., Oswald, R., Paasonen, P., Petäjä, T., Regelin, E., Sander, R., Sinha, V., Sipilä, M., Taraborrelli, D., Tatum Ernest, C., Williams, J., Lelieveld, J., and Harder, H.: Observation and modelling of HO_x radicals in a boreal forest, Atmospheric Chemistry and Physics, 14, 8723–8747, https://doi.org/10.5194/ACP-14-8723-2014, 2014.

Herrmann, H., Schaefer, T., Tilgner, A., Styler, S. A., Weller, C., Teich, M., and Otto, T.: Tropospheric Aqueous-Phase Chemistry: Kinetics, Mechanisms, and Its Coupling to a Changing Gas Phase, Chemical Reviews, 115, 4259–4334, https://doi.org/10.1021/cr500447k, pMID: 25950643, 2015.

Hersbach, H., Bell, B., Berrisford, P., Hirahara, S., Horányi, A., Muñoz-Sabater, J., Nicolas, J., Peubey, C., Radu, R., Schepers, D., Simmons, A., Soci, C., Abdalla, S., Abellan, X., Balsamo, G., Bechtold, P., Biavati, G., Bidlot, J., Bonavita, M., Chiara, G., Dahlgren, P., Dee, D., Diamantakis, M., Dragani, R., Flemming, J., Forbes, R., Fuentes, M., Geer, A., Haimberger, L., Healy, S., Hogan, R. J., Hólm, E., Janisková, M., Keeley, S., Laloyaux, P., Lopez, P., Lupu, C., Radnoti, G., Rosnay, P., Rozum, I., Vamborg, F., Villaume, S., and Thépaut, J.-N.: The ERA5 global reanalysis, Quarterly Journal of the Royal Meteorological Society, 146, 1999–2049, https://doi.org/10.1002/qj.3803, 2020.

Jagiella, S. and Zabel, F.: Reaction of phenylperoxy radicals with NO2 at 298 K, Phys. Chem. Chem. Phys., 9, 5036–5051, https://doi.org/10.1039/B705193J, 2007.

Jiménez-Muñoz, J. C., Mattar, C., Barichivich, J., Santamaría-Artigas, A., Takahashi, K., Malhi, Y., Sobrino, J. A., and Schrier, G. v. d.: Record-breaking warming and extreme drought in the Amazon rainforest during the course of El Niño 2015–2016, Scientific Reports, 6, 33 130, https://doi.org/10.1038/srep33130, 2016.

Jöckel, P., Tost, H., Pozzer, A., Brühl, C., Buchholz, J., Ganzeveld, L., Hoor, P., Kerkweg, A., Lawrence, M. G., Sander, R., Steil, B., Stiller, G., Tanarhte, M., Taraborrelli, D., van Aardenne, J., and Lelieveld, J.: The atmospheric chemistry general circulation model ECHAM5/MESSy1: consistent simulation of ozone from the surface to the mesosphere, Atmospheric Chemistry and Physics, 6, 5067–5104, https://doi.org/10.5194/acp-6-5067-2006, 2006.

Jöckel, P., Kerkweg, A., Pozzer, A., Sander, R., Tost, H., Riede, H., Baumgaertner, A., Gromov, S., and Kern, B.: Development cycle 2 of the Modular Earth Submodel System (MESSy2), Geoscientific Model Development, 3, 717–752, https://doi.org/10.5194/gmd-3-717-2010, 2010.

Jöckel, P., Tost, H., Pozzer, A., Kunze, M., Kirner, O., Brenninkmeijer, C. A. M., Brinkop, S., Cai, D. S., Dyroff, C., Eckstein, J., Frank, F., Garny, H., Gottschaldt, K.-D., Graf, P., Grewe, V., Kerkweg, A., Kern, B., Matthes, S., Mertens, M., Meul, S., Neumaier, M., Nützel, M., Oberländer-Hayn, S., Ruhnke, R., Runde, T., Sander, R., Scharffe, D., and Zahn, A.: Earth System Chemistry integrated Mod-

https://doi.org/10.5194/acp-2020-1130
Preprint. Discussion started: 17 November 2020


Atmospheric Chemistry and Physics Discussions

elling (ESCiMo) with the Modular Earth Submodel System (MESSy) version 2.51, Geoscientific Model Development, 9, 1153–1200, https://doi.org/10.5194/gmd-9-1153-2016, 2016.

Jülich Supercomputing Centre: JUWELS: Modular Tier-0/1 Supercomputer at the Jülich Supercomputing Centre, Journal of large-scale research facilities, 5, https://doi.org/10.17815/jlsrf-5-171, 2019.

Kaiser, J. W., Heil, A., Andreae, M. O., Benedetti, A., Chubarova, N., Jones, L., Morcrette, J.-J., Razinger, M., Schultz, M. G., Suttie, M., and van der Werf, G. R.: Biomass burning emissions estimated with a global fire assimilation system based on observed fire radiative power, Biogeosciences, 9, 527–554, https://doi.org/10.5194/bg-9-527-2012, 2012.

Kim, P. S., Jacob, D. J., Mickley, L. J., Koplitz, S. N., Marlier, M. E., DeFries, R. S., Myers, S. S., Chew, B. N., and Mao, Y. H.: Sensitivity of population smoke exposure to fire locations in Equatorial Asia, Atmospheric Environment, 102, 11 – 17, https://doi.org/10.1016/j.atmosenv.2014.09.045, 2015.

Koss, A. R., Sekimoto, K., Gilman, J. B., Selimovic, V., Coggon, M. M., Zarzana, K. J., Yuan, B., Lerner, B. M., Brown, S. S., Jimenez, J. L., Krechmer, J., Roberts, J. M., Warneke, C., Yokelson, R. J., and de Gouw, J.: Non-methane organic gas emissions from biomass burning: identification, quantification, and emission factors from PTR-ToF during the FIREX 2016 laboratory experiment, Atmospheric Chemistry and Physics, 18, 3299–3319, https://doi.org/10.5194/acp-18-3299-2018, 2018.

Kyrölä, E., Laine, M., Sofieva, V., Tamminen, J., Päivärinta, S.-M., Tukiainen, S., Zawodny, J., and Thomason, L.: Combined SAGE II—GOMOS ozone profile data set for 1984–2011 and trend analysis of the vertical distribution of ozone, Atmospheric Chemistry and Physics, 13, 10 645–10 658, https://doi.org/10.5194/acp-13-10645-2013, 2013.

Lee, D., Pitari, G., Grewe, V., Gierens, K., Penner, J., Petzold, A., Prather, M., Schumann, U., Bais, A., Berntsen, T., Iachetti, D., Lim, L., and Sausen, R.: Transport impacts on atmosphere and climate: Aviation, Atmospheric Environment, 44, 4678 – 4734, https://doi.org/10.1016/j.atmosenv.2009.06.005, transport Impacts on Atmosphere and Climate: The ATTICA Assessment Report, 2010.

Lee, H.-H., Bar-Or, R. Z., and Wang, C.: Biomass burning aerosols and the low-visibility events in Southeast Asia, Atmospheric Chemistry and Physics, 17, 965–980, https://doi.org/10.5194/acp-17-965-2017, 2017.

Lelieveld, J., Bourtsoukidis, E., Brühl, C., Fischer, H., Fuchs, H., Harder, H., Hofzumahaus, A., Holland, F., Marno, D., Neumaier, M., Pozzer, A., Schlager, H., Williams, J., Zahn, A., and Ziereis, H.: The South Asian monsoon—pollution pump and purifier, Science, 361, 270–273, https://doi.org/10.1126/science.aar2501, 2018.

Leslie, M. D., Ridoli, M., Murphy, J. G., and Borduas-Dedekind, N.: Isocyanic acid (HNCO) and its fate in the atmosphere: a review, Environ. Sci.: Processes Impacts, 21, 793–808, https://doi.org/10.1039/C9EM00003H, 2019.

Leuenberger, C., Ligocki, M. P., and Pankow, J. F.: Trace organic compounds in rain. 4. Identities, concentrations, and scavenging mechanisms for phenols in urban air and rain, Environmental Science & Technology, 19, 1053–1058, https://doi.org/10.1021/es00141a005, pMID: 22288749, 1985.

Li, Q., Jacob, D. J., Bey, I., Yantosca, R. M., Zhao, Y., Kondo, Y., and Notholt, J.: Atmospheric hydrogen cyanide (HCN): Biomass burning source, ocean sink?, Geophysical Research Letters, 27, 357–360, https://doi.org/10.1029/1999GL010935, 2000.

Li, Q., Palmer, P. I., Pumphrey, H. C., Bernath, P., and Mahieu, E.: What drives the observed variability of HCN in the troposphere and lower stratosphere?, Atmospheric Chemistry and Physics, 9, 8531–8543, https://doi.org/10.5194/acp-9-8531-2009, 2009.

Liu, T., Mickley, L. J., Marlier, M. E., DeFries, R. S., Khan, M. F., Latif, M. T., and Karambelas, A.: Diagnosing spatial biases and uncertainties in global fire emissions inventories: Indonesia as regional case study, Remote Sensing of Environment, 237, 111 557, https://doi.org/10.1016/j.rse.2019.111557, 2020.

https://doi.org/10.5194/acp-2020-1130
Preprint. Discussion started: 17 November 2020

Atmospheric Chemistry and Physics Discussions

Lobert, J. M., Scharffe, D. H., Hao, W. M., and Crutzen, P. J.: Importance of biomass burning in the atmospheric budgets of nitrogen-containing gases, Nature, 346, 552–554, https://doi.org/10.1038/346552a0, 1990.

Mahowald, N. M., Rasch, P. J., Eaton, B. E., Whittlestone, S., and Prinn, R. G.: Transport of 222radon to the remote troposphere using the Model of Atmospheric Transport and Chemistry and assimilated winds from ECMWF and the National Center for Environmental Prediction/NCAR, Journal of Geophysical Research: Atmospheres, 102, 28 139–28 151, https://doi.org/10.1029/97JD02084, 1997.

Marlier, M. E., DeFries, R. S., Voulgarakis, A., Kinney, P. L., Randerson, J. T., Shindell, D. T., Chen, Y., and Faluvegi, G.: El Niño and health risks from landscape fire emissions in southeast Asia, Nature Climate Change, 3, 131–136, https://doi.org/10.1038/nclimate1658, 2013.

Millet, D. B., Jacob, D. J., Custer, T. G., de Gouw, J. A., Goldstein, A. H., Karl, T., Singh, H. B., Sive, B. C., Talbot, R. W., Warneke, C., and Williams, J.: New constraints on terrestrial and oceanic sources of atmospheric methanol, Atmospheric Chemistry and Physics, 8, 6887–6905, https://doi.org/10.5194/acp-8-6887-2008, 2008.

Molina, M. J. and Rowland, F. S.: Stratospheric sink for chlorofluoromethanes: chlorine atom-catalysed destruction of ozone, Nature, 249, 810–812, https://doi.org/10.1038/249810a0, 1974.

Nair, P. J., Froidevaux, L., Kuttippurath, J., Zawodny, J. M., Russell III, J. M., Steinbrecht, W., Claude, H., Leblanc, T., van Gijsel, J. A. E., Johnson, B., Swart, D. P. J., Thomas, A., Querel, R., Wang, R., and Anderson, J.: Subtropical and midlatitude ozone trends in the stratosphere: Implications for recovery, Journal of Geophysical Research: Atmospheres, 120, 7247–7257, https://doi.org/10.1002/2014JD022371, 2015.

Natangelo, M., Mangiapan, S., Bagnati, R., Benfenati, E., and Fanelli, R.: Increased concentrations of nitrophenols in leaves from a damaged forestal site, Chemosphere, 38, 1495 – 1503, https://doi.org/10.1016/S0045-6535(98)00370-1, 1999.

Nechita-Banda, N., Krol, M., van der Werf, G. R., Kaiser, J. W., Pandey, S., Huijnen, V., Clerbaux, C., Coheur, P., Deeter, M. N., and Röckmann, T.: Monitoring emissions from the 2015 Indonesian fires using CO satellite data, Philosophical Transactions of the Royal Society B: Biological Sciences, 373, 20170 307, https://doi.org/10.1098/rstb.2017.0307, 2018.

NOAA: Multivariate ENSO Index Version 2 (MEI.v2), https://psl.noaa.gov/enso/mei/, (last accessed 19 September 2020), 2020.

Nojima, K., Fukaya, K., Fukui, S., and Kanno, S.: Studies on photochemistry of aromatic hydrocarbons II: The formation of nitrophenols and nitrobenzene by the photochemical reaction of benzene in the presence of nitrogen monoxide, Chemosphere, 4, 77–82, 1975.

Nölscher, A., Butler, T., Auld, J., Veres, P., Muñoz, A., Taraborrelli, D., Vereecken, L., Lelieveld, J., and Williams, J.: Using total OH reactivity to assess isoprene photooxidation via measurement and model, Atmos. Environ., 89, 453–463, https://doi.org/10.1016/j.atmosenv.2014.02.024, 2014.

Orbe, C., Yang, H., Waugh, D. W., Zeng, G., Morgenstern, O., Kinnison, D. E., Lamarque, J.-F., Tilmes, S., Plummer, D. A., Scinocca, J. F., Josse, B., Marecal, V., Jöckel, P., Oman, L. D., Strahan, S. E., Deushi, M., Tanaka, T. Y., Yoshida, K., Akiyoshi, H., Yamashita, Y., Stenke, A., Revell, L., Sukhodolov, T., Rozanov, E., Pitari, G., Visioni, D., Stone, K. A., Schofield, R., and Banerjee, A.: Large-scale tropospheric transport in the Chemistry–Climate Model Initiative (CCMI) simulations, Atmospheric Chemistry and Physics, 18, 7217–7235, https://doi.org/10.5194/acp-18-7217-2018, 2018.

Park, M., Randel, W. J., Emmons, L. K., Bernath, P. F., Walker, K. A., and Boone, C. D.: Chemical isolation in the Asian monsoon anticyclone observed in Atmospheric Chemistry Experiment (ACE-FTS) data, Atmospheric Chemistry and Physics, 8, 757–764, https://doi.org/10.5194/acp-8-757-2008, 2008.

Randel, W. J., Park, M., Emmons, L., Kinnison, D., Bernath, P., Walker, K. A., Boone, C., and Pumphrey, H.: Asian Monsoon Transport of Pollution to the Stratosphere, Science, 328, 611–613, https://doi.org/10.1126/science.1182274, 2010.

https://doi.org/10.5194/acp-2020-1130
Preprint. Discussion started: 17 November 2020

Reddington, C. L., Yoshioka, M., Balasubramanian, R., Ridley, D., Toh, Y. Y., Arnold, S. R., and Spracklen, D. V.: Contribution of vegetation and peat fires to particulate air pollution in Southeast Asia, Environmental Research Letters, 9, 094 006, https://doi.org/10.1088/1748-9326/9/9/094006, 2014.

Rein, G., Cohen, S., and Simeoni, A.: Carbon emissions from smouldering peat in shallow and strong fronts, Proceedings of the Combustion Institute, 32, 2489–2496, https://doi.org/10.1016/j.proci.2008.07.008, 2009.

Rippen, G., Zietz, E., Frank, R., Knacker, T., and Klöpffer, W.: Do airborne nitrophenols contribute to forest decline?, Environmental Technology Letters, 8, 475–482, https://doi.org/10.1080/09593338709384508, 1987.

Roberts, J. M., Veres, P. R., Cochran, A. K., Warneke, C., Burling, I. R., Yokelson, R. J., Lerner, B., Gilman, J. B., Kuster, W. C., Fall, R., and de Gouw, J.: Isocyanic acid in the atmosphere and its possible link to smoke-related health effects, Proceedings of the National Academy of Sciences, 108, 8966–8971, https://doi.org/10.1073/pnas.1103352108, 2011.

Roeckner, E., Brokopf, R., Esch, M., Giorgetta, M., Hagemann, S., Kornblueh, L., Manzini, E., Schlese, U., and Schulzweida, U.: Sensitivity of Simulated Climate to Horizontal and Vertical Resolution in the ECHAM5 Atmosphere Model, Journal of Climate, 19, 3771–3791, https://doi.org/10.1175/JCLI3824.1, 2006.

Rosanka, S., Frömming, C., and Grewe, V.: The impact of weather patterns and related transport processes on aviation's contribution to ozone and methane concentrations from NO_x emissions, Atmospheric Chemistry and Physics, 20, 12 347–12 361, https://doi.org/10.5194/acp-20-12347-2020, 2020a.

Rosanka, S., Sander, R., Franco, B., Wespes, C., Wahner, A., and Taraborrelli, D.: Oxidation of low-molecular weight organic compounds in cloud droplets: global impact on tropospheric oxidants, Atmospheric Chemistry and Physics Discussions, 2020, 1–33, https://doi.org/10.5194/acp-2020-1041, 2020b.

Rosanka, S., Sander, R., Wahner, A., and Taraborrelli, D.: Oxidation of low-molecular weight organic compounds in cloud droplets: development of the JAMOC chemical mechanism in CAABA/MECCA (version 4.5.0gmdd), Geoscientific Model Development Discussions, 2020, 1–18, https://doi.org/10.5194/gmd-2020-337, 2020c.

Rosanka, S., Vu, G. H. T., Nguyen, H. M. T., Pham, T. V., Javed, U., Taraborrelli, D., and Vereecken, L.: Atmospheric chemical loss processes of isocyanic acid (HNCO): a combined theoretical kinetic and global modelling study, Atmospheric Chemistry and Physics, 20, 6671–6686, https://doi.org/10.5194/acp-20-6671-2020, 2020d.

Sander, R., Baumgaertner, A., Cabrera-Perez, D., Frank, F., Gromov, S., Grooß, J.-U., Harder, H., Huijnen, V., Jöckel, P., Karydis, V. A., Niemeyer, K. E., Pozzer, A., Riede, H., Schultz, M. G., Taraborrelli, D., and Tauer, S.: The community atmospheric chemistry box model CAABA/MECCA-4.0, Geoscientific Model Development, 12, 1365–1385, https://doi.org/10.5194/gmd-12-1365-2019, 2019.

Schummer, C., Groff, C., Al Chami, J., Jaber, F., and Millet, M.: Analysis of phenols and nitrophenols in rainwater collected simultaneously on an urban and rural site in east of France, Science of The Total Environment, 407, 5637 – 5643, https://doi.org/10.1016/j.scitotenv.2009.06.051, 2009.

Shim, C., Wang, Y., Singh, H. B., Blake, D. R., and Guenther, A. B.: Source characteristics of oxygenated volatile organic compounds and hydrogen cyanide, Journal of Geophysical Research: Atmospheres, 112, https://doi.org/10.1029/2006JD007543, 2007.

Sindelarova, K., Granier, C., Bouarar, I., Guenther, A., Tilmes, S., Stavrakou, T., Müller, J.-F., Kuhn, U., Stefani, P., and Knorr, W.: Global data set of biogenic VOC emissions calculated by the MEGAN model over the last 30 years, Atmospheric Chemistry and Physics, 14, 9317–9341, https://doi.org/10.5194/acp-14-9317-2014, 2014.

Singh, H. B., Salas, L., Herlth, D., Kolyer, R., Czech, E., Viezee, W., Li, Q., Jacob, D. J., Blake, D., Sachse, G., Harward, C. N., Fuelberg, H., Kiley, C. M., Zhao, Y., and Kondo, Y.: In situ measurements of HCN and CH3CN over the Pacific Ocean: Sources, sinks, and budgets, Journal of Geophysical Research: Atmospheres, 108, https://doi.org/10.1029/2002JD003006, 2003.

Smith, T. E. L., Evers, S., Yule, C. M., and Gan, J. Y.: In Situ Tropical Peatland Fire Emission Factors and Their Variability, as Determined by Field Measurements in Peninsula Malaysia, Global Biogeochemical Cycles, 32, 18–31, https://doi.org/10.1002/2017GB005709, 2018.

Stockwell, C. E., Veres, P. R., Williams, J., and Yokelson, R. J.: Characterization of biomass burning emissions from cooking fires, peat, crop residue, and other fuels with high-resolution proton-transfer-reaction time-of-flight mass spectrometry, Atmospheric Chemistry and Physics, 15, 845–865, https://doi.org/10.5194/acp-15-845-2015, 2015.

Stockwell, C. E., Jayarathne, T., Cochrane, M. A., Ryan, K. C., Putra, E. I., Saharjo, B. H., Nurhayati, A. D., Albar, I., Blake, D. R., Simpson, I. J., Stone, E. A., and Yokelson, R. J.: Field measurements of trace gases and aerosols emitted by peat fires in Central Kalimantan, Indonesia, during the 2015 El Niño, Atmospheric Chemistry and Physics, 16, 11 711–11 732, https://doi.org/10.5194/acp-16-11711-2016, 2016.

Strahan, S. E. and Douglass, A. R.: Decline in Antarctic Ozone Depletion and Lower Stratospheric Chlorine Determined From Aura Microwave Limb Sounder Observations, Geophysical Research Letters, 45, 382–390, https://doi.org/10.1002/2017GL074830, 2018.

Tao, Z. and Li, Z.: A kinetics study on reactions of C6H5O with C6H5O and O3 at 298 k, International Journal of Chemical Kinetics, 31, 65–72, https://doi.org/10.1002/(SICI)1097-4601(1999)31:1<65::AID-KIN8>3.0.CO;2-J, 1999.

Taraborrelli, D., Lawrence, M. G., Butler, T. M., Sander, R., and Lelieveld, J.: Mainz Isoprene Mechanism 2 (MIM2): an isoprene oxidation mechanism for regional and global atmospheric modelling, Atmospheric Chemistry and Physics, 9, 2751–2777, https://doi.org/10.5194/ACP-9-2751-2009, 2009.

Taraborrelli, D., Lawrence, M. G., Crowley, J. N., Dillon, T. J., Gromov, S., Groß, C. B. M., Vereecken, L., and Lelieveld, J.: Hydroxyl radical buffered by isoprene oxidation over tropical forests, Nature Geoscience, 5, 190–193, https://doi.org/10.1038/ngeo1405, 2012.

Taraborrelli, D., Cabrera-Perez, D., Bacer, S., Gromov, S., Lelieveld, J., Sander, R., and Pozzer, A.: Influence of aromatics on tropospheric gas-phase composition, Atmospheric Chemistry and Physics Discussions, 2020, 1–26, https://doi.org/10.5194/acp-2020-461, 2020.

Tost, H., Jöckel, P., Kerkweg, A., Sander, R., and Lelieveld, J.: Technical note: A new comprehensive SCAVenging submodel for global atmospheric chemistry modelling, Atmospheric Chemistry and Physics, 6, 565–574, https://doi.org/10.5194/acp-6-565-2006, 2006.

Trenberth, K. E.: The Definition of El Niño, Bulletin of the American Meteorological Society, 78, 2771–2778, https://doi.org/10.1175/1520-0477(1997)078<2771:TDOENO>2.0.CO;2, 1997.

United Nations, Department of Economic and Social Affairs, Population Division: World Population Prospects 2019: Data Booklet, https://population.un.org/wpp/Publications/Files/WPP2019_DataBooklet.pdf, ST/ESA/SER.A/424, 2019.

van der Werf, G. R., Randerson, J. T., Giglio, L., van Leeuwen, T. T., Chen, Y., Rogers, B. M., Mu, M., van Marle, M. J. E., Morton, D. C., Collatz, G. J., Yokelson, R. J., and Kasibhatla, P. S.: Global fire emissions estimates during 1997–2016, Earth System Science Data, 9, 697–720, https://doi.org/10.5194/essd-9-697-2017, 2017.

Vereecken, L., Chakravarty, H. K., Bohn, B., and Lelieveld, J.: Theoretical Study on the Formation of H- and O-Atoms, HONO, OH, NO, and NO2 from the Lowest Lying Singlet and Triplet States in Ortho-Nitrophenol Photolysis, International Journal of Chemical Kinetics, 48, 785–795, https://doi.org/10.1002/kin.21033, 2016.

Vigouroux, C., Blumenstock, T., Coffey, M., Errera, Q., García, O., Jones, N. B., Hannigan, J. W., Hase, F., Liley, B., Mahieu, E., Mellqvist, J., Notholt, J., Palm, M., Persson, G., Schneider, M., Servais, C., Smale, D., Thölix, L., and De Mazière, M.: Trends of ozone total columns

and vertical distribution from FTIR observations at eight NDACC stations around the globe, Atmospheric Chemistry and Physics, 15, 2915–2933, https://doi.org/10.5194/acp-15-2915-2015, 2015.

Vogel, B., Günther, G., Müller, R., Grooß, J.-U., and Riese, M.: Impact of different Asian source regions on the composition of the Asian monsoon anticyclone and of the extratropical lowermost stratosphere, Atmospheric Chemistry and Physics, 15, 13 699–13 716, https://doi.org/10.5194/acp-15-13699-2015, 2015.

Walker, J. C., Dudhia, A., and Carboni, E.: An effective method for the detection of trace species demonstrated using the MetOp Infrared Atmospheric Sounding Interferometer, Atmospheric Measurement Techniques, 4, 1567–1580, https://doi.org/10.5194/amt-4-1567-2011, 2011.

Wang, Z., Nicholls, S. J., Rodriguez, E. R., Kummu, O., Hörkkö, S., Barnard, J., Reynolds, W. F., Topol, E. J., DiDonato, J. A., and Hazen, S. L.: Protein carbamylation links inflammation, smoking, uremia and atherogenesis, Nature Medicine, 13, 1176–1184, https://doi.org/10.1038/nm1637, 2007.

Weng, H., Ashok, K., Behera, S. K., Rao, S. A., and Yamagata, T.: Impacts of recent El Niño Modoki on dry/wet conditions in the Pacific rim during boreal summer, Climate Dynamics, 29, 113–129, https://doi.org/10.1007/s00382-007-0234-0, 2007.

Whitburn, S., Van Damme, M., Clarisse, L., Bauduin, S., Heald, C. L., Hadji-Lazaro, J., Hurtmans, D., Zondlo, M. A., Clerbaux, C., and Coheur, P.-F.: A flexible and robust neural network IASI-NH3 retrieval algorithm, Journal of Geophysical Research: Atmospheres, 121, 6581–6599, https://doi.org/10.1002/2016jd024828, 2016a.

Whitburn, S., Van Damme, M., Clarisse, L., Turquety, S., Clerbaux, C., and Coheur, P.-F.: Doubling of annual ammonia emissions from the peat fires in Indonesia during the 2015 El Niño, Geophysical Research Letters, 43, 11,007–11,014, https://doi.org/10.1002/2016gl070620, 2016b.

Xu, J., Morris, P. J., Liu, J., and Holden, J.: PEATMAP: Refining estimates of global peatland distribution based on a meta-analysis, https://doi.org/10.5518/252, (Dataset), 2017.

Xu, J., Morris, P. J., Liu, J., and Holden, J.: PEATMAP: Refining estimates of global peatland distribution based on a meta-analysis, CATENA, 160, 134 – 140, https://doi.org/10.1016/j.catena.2017.09.010, 2018.

Yu, Z., Loisel, J., Brosseau, D. P., Beilman, D. W., and Hunt, S. J.: Global peatland dynamics since the Last Glacial Maximum, Geophysical Research Letters, 37, https://doi.org/10.1029/2010GL043584, 2010.

Yuan, C., Lau, W. K. M., Li, Z., and Cribb, M.: Relationship between Asian monsoon strength and transport of surface aerosols to the Asian Tropopause Aerosol Layer (ATAL): interannual variability and decadal changes, Atmospheric Chemistry and Physics, 19, 1901–1913, https://doi.org/10.5194/acp-19-1901-2019, 2019.

Zhang, C.: Madden–Julian Oscillation: Bridging Weather and Climate, Bulletin of the American Meteorological Society, 94, 1849–1870, https://doi.org/10.1175/BAMS-D-12-00026.1, 2013.

Zhang, K., Wan, H., Zhang, M., and Wang, B.: Evaluation of the atmospheric transport in a GCM using radon measurements: sensitivity to cumulus convection parameterization, Atmospheric Chemistry and Physics, 8, 2811–2832, https://doi.org/10.5194/acp-8-2811-2008, 2008.